

# 1 Versatile soil gas concentration and isotope monitoring: optimization 2 and integration of novel soil gas probes with online trace gas 3 detection

4 Juliana Gil-Loaiza<sup>1</sup>, Joseph R. Roscioli<sup>2</sup>, Joanne H. Shorter<sup>2</sup>, Till H. M. Volkmann<sup>3,4</sup>, Wei-Ren Ng<sup>3</sup>,  
5 Jordan E. Krechmer<sup>2</sup>, Laura K. Meredith<sup>1,3,\*</sup>

6  
7 <sup>1</sup>School of Natural Resources and the Environment, University of Arizona, Tucson, AZ, 85721, USA

8 <sup>2</sup>Aerodyne Research Inc., Billerica, MA, 01821, USA

9 <sup>3</sup>Biosphere 2, University of Arizona, Oracle, AZ, 85623, USA

10 <sup>4</sup>Applied Intelligence, Accenture, Kronberg im Taunus, Hesse, 61476, Germany.

11 *Correspondence to:* Laura K. Meredith [laurameredith@email.arizona.edu](mailto:laurameredith@email.arizona.edu)

12 **Abstract.** Gas concentrations and isotopic signatures can unveil microbial metabolisms and their responses to environmental  
13 changes in soil. Currently, few methods measure in situ soil trace gases such as the products of nitrogen and carbon cycling,  
14 or volatile organic compounds (VOCs) that constrain microbial biochemical processes like nitrification, methanogenesis,  
15 respiration, and microbial communication. Versatile trace gas sampling systems that integrate soil probes with sensitive trace  
16 gas analyzers could fill this gap with in situ soil gas measurements that resolve spatial (centimeters) and temporal (minutes)  
17 patterns. We developed a system that integrates new porous and hydrophobic sintered PTFE diffusive soil gas probes that non-  
18 disruptively collect soil gas samples with a transfer system to directs gas from multiple probes to one or more central gas  
19 analyzer(s) such as laser and mass spectrometers. Here, we demonstrate the feasibility and versatility of this automated multi-  
20 probe system for soil gas measurements of isotopic ratios of nitrous oxide ( $\delta^{18}\text{O}$ ,  $\delta^{15}\text{N}$ , and the  $^{15}\text{N}$  site-preference of  $\text{N}_2\text{O}$ ),  
21 methane, carbon dioxide ( $\delta^{13}\text{C}$ ), and VOCs. First, we used an inert silica matrix to challenge probe measurements under  
22 controlled gas conditions. By changing and controlling system flow parameters, including the probe flow rate, we optimized  
23 recovery of representative soil gas samples while reducing sampling artifacts on subsurface concentrations. Second, we used  
24 this system to provide a real-time window into the impact of environmental manipulations of irrigation and soil redox  
25 conditions on in situ  $\text{N}_2\text{O}$  and VOC concentrations. Moreover, to reveal the dynamics in the stable isotope ratios of  $\text{N}_2\text{O}$  (i.e.,  
26  $^{14}\text{N}^{14}\text{N}^{16}\text{O}$ ,  $^{14}\text{N}^{15}\text{N}^{16}\text{O}$ ,  $^{15}\text{N}^{14}\text{N}^{16}\text{O}$ , and  $^{14}\text{N}^{14}\text{N}^{18}\text{O}$ ), we developed a new high-precision laser spectrometer with a reduced  
27 sample volume demand. Our system integrating TILDAS-PTR-MS Vocus in line with sPTFE soil gas probes successfully  
28 quantified isotopic signatures for  $\text{N}_2\text{O}$ ,  $\text{CO}_2$ , and VOCs in real time as response to changes in dry-wetting cycle and redox  
29 conditions.

30 Broadening the collection of trace gases that can be monitored in the subsurface is critical for monitoring biogeochemical  
31 cycles, ecosystem health, and management practices at scales relevant to the soil system.

## 32 **1 Introduction**

33 The impact of the biosphere's soils on atmospheric composition is typically measured at the soil surface, yet  
34 belowground approaches may provide a more mechanistic perspective into trace gas cycling. Soil is a source and sink of trace  
35 gases such as nitrous oxide (N<sub>2</sub>O), carbon dioxide (CO<sub>2</sub>), methane (CH<sub>4</sub>), and volatile organic compounds (VOCs) that impact  
36 climate and air quality. Soil fluxes are driven by abiotic and biotic processes including microbial metabolism and soil  
37 environmental conditions (Conrad, 2005; Karbin et al., 2015; Jiao et al., 2018) that vary in space (i.e. soil aggregate (Schimel,  
38 2018) to field (Wang et al., 2014)) and time (e.g. rain-driven emission pulses)(Jiao et al., 2018). Environmental drivers such  
39 as soil moisture and oxygen availability modulate rates of aerobic and anaerobic processes that influence gas cycling including  
40 N<sub>2</sub>O emissions (Groffman et al., 2009) and VOC fluxes (Raza et al., 2017; Abis et al., 2020). Yet, capturing how belowground  
41 variations in soil structure (e.g., air-filled soil porosity) and conditions (e.g., moisture, wetting frequency, redox state) impact  
42 gas cycling remains challenging. While surface flux chambers remain a dominant, integrative tool to constrain soil gas fluxes,  
43 new capabilities are needed to unearth spatiotemporal variations in belowground processes.

44 Soil gases serve as messengers of belowground biogeochemical processes and microbial activity. Soil microbes  
45 produce trace gases via biochemical pathways that impart characteristic isotopic signatures onto trace gases that help identify  
46 and quantify gas processes (Yoshida and Toyoda, 2000). For example, microbial pathways driving CH<sub>4</sub> production have been  
47 identified from the ratio of rare <sup>13</sup>CH<sub>4</sub> to the abundant <sup>12</sup>CH<sub>4</sub> natural isotopes (McCalley et al., 2014; Penger et al., 2012). Other  
48 studies use isotopically enriched trace gases, such as <sup>15</sup>N-N<sub>2</sub>O to determine consumption and production rates of N<sub>2</sub>O in soil  
49 columns (Clough et al., 2006). The ratio of <sup>15</sup>N to <sup>14</sup>N, and the position of the <sup>15</sup>N relative to the O in N<sub>2</sub>O (termed the <sup>15</sup>N site  
50 preference) depends on the N<sub>2</sub>O production pathway (Yoshida and Toyoda, 2000; Sutka et al., 2006), with the <sup>15</sup>N site  
51 preference reflecting only the microbial pathway and not substrate isotopic signature. Together, measurements of all three  
52 isotopic properties of N<sub>2</sub>O (<sup>15</sup>N abundance, <sup>15</sup>N site preference, and <sup>18</sup>O abundance) can identify the type of biochemical  
53 process generating the N<sub>2</sub>O, and the associated microbial groups (bacterial, archaeal, or fungal) (Toyoda et al., 2017). VOCs  
54 are signals for diverse microbial and chemical interactions in soils that are increasingly recognized as an important part of the  
55 soil metabolome (Honeker et al., 2021). VOCs are also involved in microbial and plant-microbe interactions such as quorum  
56 sensing, and they may reflect soil health, stress responses, and microbial identity (Insam and Seewald, 2010; Schulz-Bohm et  
57 al., 2018). Inert tracers present or released in soil (e.g., Helium (Laemmel et al., 2017)) help distinguish physical from chemical  
58 mechanisms affecting soil gas concentrations. Tracking microbial activity using trace gas messengers can elevate the  
59 understanding of the role of microbial communities and their metabolism in soil.

60 Soil gas sampling approaches have evolved to recover gas samples with less disruption to the soil environment. Early  
61 methods inserted rigid perforated tubes or wells into the soil to withdraw gas by suction using a syringe (Holter, 1990), pump

62 (Maier et al., 2012), or other manual methods (Panikov et al., 2007). This methodology was time consuming, created artifacts  
63 by driving advective flow that transports gas from other regions and disturbed the probe surroundings (Maier et al., 2012). In  
64 contrast, diffusive probes sample soil gases by non-advective gas exchange driven by molecular diffusion across a porous  
65 membrane from soil gas and aqueous phase partitioning (Volkman et al., 2016a, 2016b). One drawback of diffusive sampling  
66 probes has been their relatively large volume, which was used to generate sufficient sample for gas analyzers, but led to  
67 correspondingly long times for the internal sampling volume to reach equilibration with soil gas. For example, probes longer  
68 than 1 m have been used in water (Rothfuss et al., 2013) and soil (Jacinthe and Dick, 1996), and small silicone probes require  
69 extended sampling return periods (>7–48 hours) to equilibrate (Kammann et al., 2001) (Petersen, 2014). Long probes disturb  
70 soil, especially upon installation, spurring the interest in discovering new materials that enhance diffusion at a smaller probe  
71 size while still resolving gas concentrations and isotopic signatures. Polypropylene (Accurel, V8/2HF, Membrana GmbH,  
72 Germany) materials have improved equilibrium time at an equivalent probe length (Flechard et al., 2007; Gut et al., 1998;  
73 Rothfuss et al., 2015), for example, Rothfuss et al., 2015 used a 15 cm PP tubing to measure water isotope for 290 days. High  
74 density materials like expanded polytetrafluoroethylene (PTFE) and polyethylene equilibrate faster than silicone (DeSutter et  
75 al., 2006), increasing temporal resolution from hours to minutes in different matrices including for the analysis of water  
76 isotopes in soil (Volkman and Weiler, 2014) and tree xylem (Volkman et al., 2016a) and CO<sub>2</sub> in soil (DeSutter et al., 2006).  
77 The diffusive sampling approach is a promising means for non-destructively recovering soil gas for analysis, despite challenges  
78 in finding porous materials that equilibrate efficiently with minimal probe length.

79 Probes face multiple demands in the soil system during field deployment. For long-term monitoring in the field,  
80 subsurface probes must be robust to extreme weather, plant and microbial activity, and disruptions that could affect the integrity  
81 of the porous membrane. While current materials recover representative gas concentrations and isotopic signatures, their  
82 application has been limited by cracking, water infiltration (Volkman et al., 2016a, 2016b), and soil disruption during  
83 sampling (Hirsch et al., 2004). Microbial interactions with probe materials can reduce probe integrity, modify gas  
84 concentrations, or reduce gas exchange by biofouling (Krämer and Conrad, 1993). Small soil particles can clog pores and limit  
85 gas diffusion, and probes can break or crack in freeze-thaw cycles (Burton and Beauchamp, 1994; Gut et al., 1998) or during  
86 installation (Volkman et al., 2016a, 2016b). Probe membranes must resist water break-through, which has caused water  
87 interference problems in nylon (Burton and Beauchamp, 1994) and polypropylene (Gut et al., 1998) probes. The limitations  
88 of some probe materials have been evaluated under controlled conditions (DeSutter et al., 2006; Munksgaard et al., 2011;  
89 Rothfuss et al., 2013). To meet the demands of long-term soil sampling, new non-reactive and hydrophobic porous probe  
90 materials are needed.

91 Diffusive soil gas probes can be integrated with online gas analyzers (e.g., for H<sub>2</sub>O, CO<sub>2</sub>, CH<sub>4</sub>) to quantify soil gas  
92 concentrations and isotopic signatures (Gangi et al., 2015; Gut et al., 1998; Rothfuss et al., 2013; Volkman et al., 2016b,  
93 2018). Growing capabilities in trace gas analysis can be leveraged to monitor additional tracers of subsurface processes. For  
94 example, small molecules such as N<sub>2</sub>O, CH<sub>4</sub>, NO, CO<sub>2</sub>, and CO can be monitored using Tunable Infrared Laser Direct  
95 Absorption Spectrometry (TILDAS) and VOCs are now routinely monitored by Proton Transfer Reaction Time Of Flight Mass

96 Spectrometers (PTR-TOF-MS). For each trace gas analyte and corresponding analyzer, methods for soil gas sampling should  
97 be optimized in ways that account for differences in molecular diffusivity (exchange across probe) and surface interactions  
98 (partitioning to tubing). Sample transfer systems multiplex gas analyzers with multiple soil probes for online measurements of  
99 multiple spatial points (Jochheim et al., 2018; Volkman and Weiler, 2014). Expanding the suite of gases that can be sampled  
100 by diffusive soil probes will enhance spatiotemporal resolution of observable interactions between microbial activity and  
101 biogeochemical processes in the environment, and their interactive impact on the atmosphere.

102 In this study, we describe a real time soil trace gas sampling system that integrates diffusive soil probes with online  
103 gas analyzers (TILDAS and PTR-TOF-MS) to capture fast, spatially resolved concentrations and isotopic signatures of key  
104 soil gases and their responses to environmental changes. We expect that a minimally disruptive, diffusive soil gas probe  
105 approach would be capable of high spatiotemporal resolution measurements of soil trace gases. To test this, we developed  
106 diffusive, hydrophobic soil probes from sintered PTFE (sPTFE) and used controlled soil columns to evaluate their ability to  
107 retrieve gas samples via continuous sampling. We optimized the TILDAS sample cell volume, sample transfer schemes and  
108 flow rates, and the instrument's concentration dependence. With the optimized system, we then performed process studies in  
109 soil to determine whether the system could unveil soil microbial metabolisms and their responses to environmental changes.  
110 Soil wetting events are known to stimulate N<sub>2</sub>O emissions from soil, and we performed an irrigation manipulation on soil  
111 column and measured the subsurface site-specific stable isotopes of N<sub>2</sub>O in realtime. We hypothesized that soil wetting would  
112 induce a shift in N<sub>2</sub>O production pathways that would be detectable via the isotopic tracers. Moreover, recognizing the  
113 sensitivity of biochemical transformations to redox conditions, we measured multiple subsurface trace gases (N<sub>2</sub>O, CO<sub>2</sub>,  
114 VOCs) after changing the redox conditions in soil. We hypothesized that the dynamic response in subsurface gas  
115 concentrations would not be uniform across compounds, reflecting sensitivity of (bio)chemical reactions to soil redox state.  
116 Here, we present the optimization and application of an online soil gas sampling approach that is robust and flexible with  
117 translatability for a wide array of trace gases that reflect microbial activity and biogeochemical cycles in soils.

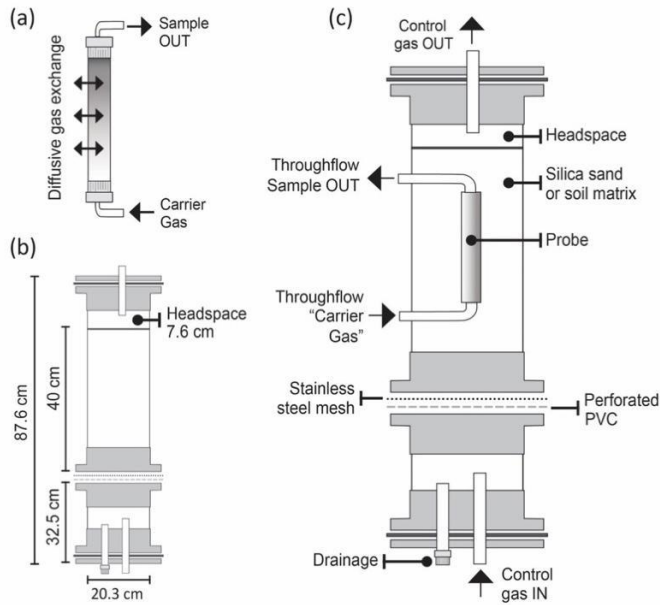
## 118 **2. Materials and Methods**

### 119 **2.1 Probes and probe evaluation system**

#### 120 **2.1.1 Sintered PTFE (sPTFE) probes**

121 We built gas permeable soil probes from microporous tubes of sPTFE (Fig. 1a). sPTFE is hydrophobic and it has  
122 uniform pore distribution, improving gas diffusion (Dhanumalayan and Joshi, 2018). The material is structurally stable and  
123 non-reactive, properties that make this material a good candidate for long term soil gas probes. We selected four probes with  
124 different pore sizes and dimensions (Table 1) to evaluate their equilibration properties. Probes were machined (White  
125 Industries, Inc., Petaluma, CA) from solid sPTFE blocks (Berghof GmbH, Eningen, Germany). We constructed probe  
126 prototype assemblies to connect probes to inlet and outlet transport lines of 1/8" fluorinated ethylene propylene (FEP,

127 Versilion™, Saint-Gobain, Malvern, PA) using stainless steel reducing unions (Swagelok, Solon, OH). In some cases, probes  
 128 were assembled from two pieces (Table 1) using perfluoroalkoxy (PFA) unions (Swagelok, Solon, OH). After assembly, probe  
 129 assembly leak-tightness at the fittings was tested by submersion under water while flowing ultra-zero air through the probe.



130

131 **Figure 1.** Gas probe and soil column assemblies. (a) microporous probe of sPTFE, (b) dimensions of the two column sections  
 132 of the custom soil column assembly built to evaluate probe performance and, (c) probe and column components for probe  
 133 evaluation.

134 **Table 1.** sPTFE probe pore size and dimensions including outer diameter (OD), inner diameter (ID), and wall thickness (W)

Probe ID (pore size in $\mu\text{m}$ )	Dimensions (mm) (OD x ID x W)	Length (mm)
P5 (5)	12.7 x 6.3 x 1.6	147.5
P8 (8)	12.7 x 6.3 x 1.6	147.5
P10 (10)	12.7 x 6.3 x 1.6	147.5
P25* (25)	9.5 x 4.7 x 2.4	147.5

135 \* Two sPTFE pieces joined with a PFA fitting

## 136 2.1.2 Soil Columns

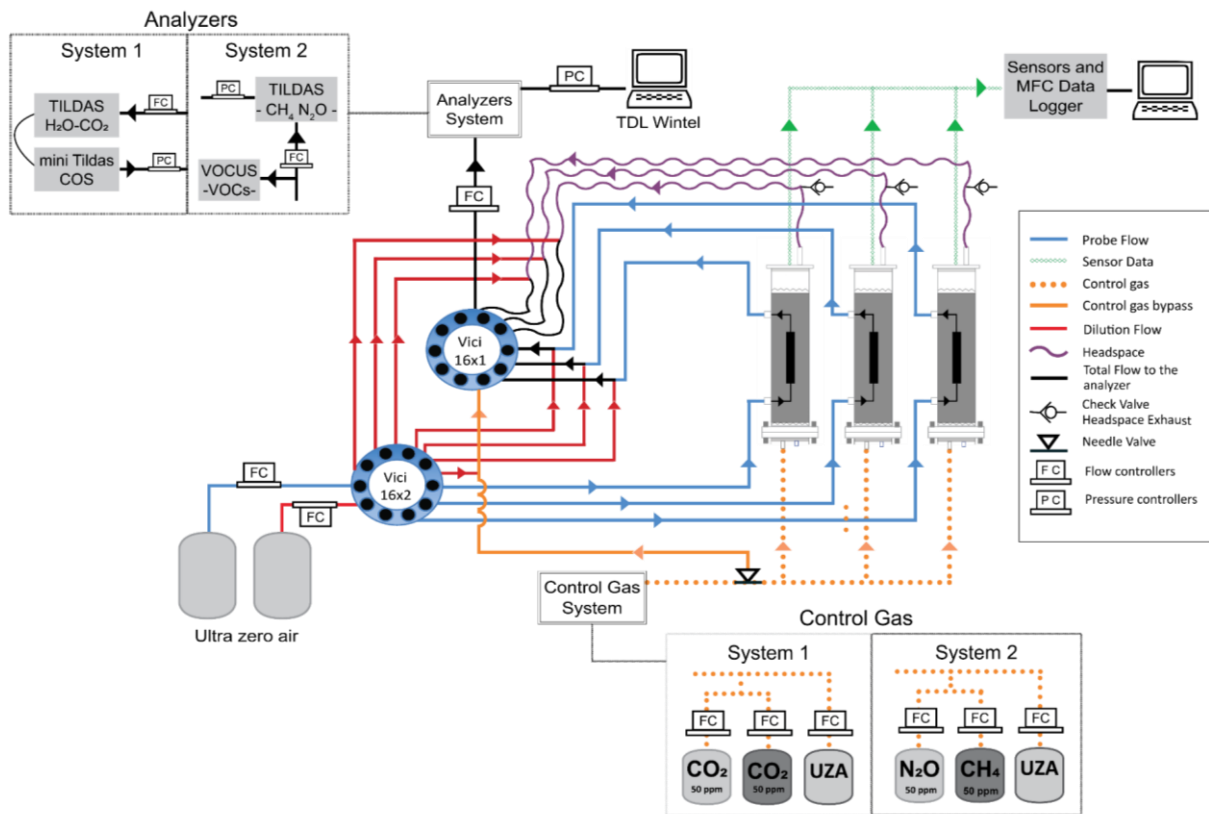
137 We used soil columns to evaluate probe performance under controlled soil gas in a non-reactive matrix (silica sand).  
138 Silica sand (Granusil 4095; high purity industrial quartz; Covia Corporation, Emmett, Idaho) was used as the non-reactive  
139 matrix, which is a low alkaline oxide matrix with a characterized particle size distribution (Table S1). We designed the column  
140 to allow a gas of controlled composition (control gas) to be advectively forced through the silica matrix from below (Fig. 1)  
141 to evaluate probe performance (System 1 tests at University of Arizona; UA, and System 2 tests at Aerodyne Research Inc.,  
142 ARI, Section 2.3.1). We also used the columns to measure in situ gas dynamics in response to environmental manipulations  
143 (e.g. wetting, redox state) in a complex matrix (soil) (System 2 tests at ARI, Section 2.3.2).

144 The lower column section (Fig. 1b) supported drainage and buffered delivery of control gas, and the upper section  
145 contained the matrix (silica or soil), with a headspace layer for uniform column outflow. Together, the two column sections  
146 had a 20.3 cm inner diameter, 87.6 cm length (including base and cover), and 28 L volume. The probe was positioned centrally  
147 in the upper section to allow sufficient distance from column walls (10 cm) and the soil/gas interface (15.2 cm) to avoid edge  
148 effects (Fig. 1c). The upper and lower column sections were separated by a layer of perforated PVC (staggered 1/8 in. holes  
149 and 40% open area) and a type 304 stainless steel wire cloth mesh (325 x 325 mesh (44  $\mu\text{m}$ ), 0.051 mm opening size) to allow  
150 passage of control gas and drainage of water (sealed during sampling), while retaining matrix integrity in the upper section.  
151 Column sections were joined using schedule-80 PVC pipes, flanges, bolts, and rubber gasket seals allowing columns to be  
152 modular and easy to disassemble, transport, and refill. Additionally, PTFE and polyetheretherketone (PEEK) bulkhead fittings  
153 (IDEX Health & Science LLC., Oak Harbor, WA, USA) and washers provided air- and water tight connections for gas tubing.  
154 Soil sensors (e.g. moisture, temperature) flanked the soil probes (Fig. 1c).

## 155 2.1.3 Gas sampling system

156 The soil probe sampling system operated in a continuous flow mode whereby carrier gas (Ultra Zero Air, UZA; Airgas  
157 Inc.) flowed through the soil probe to equilibrate with soil gas (probe flow), and the outflow was diluted online (dilution flow),  
158 and the combined flow (total flow) was sent to the gas analyzer for real time measurement. The gas sampling system consisted  
159 of a controlled soil gas transfer system, sampling probes, and a measurement and data acquisition system that coordinated  
160 sampling in three gas columns (Fig. 2). Nearly identical sampling systems were built at UA (System 1) and Aerodyne (System  
161 2) and differed in the specific TILDAS and gas control components deployed at each location (Table 2). To prevent bulk gas  
162 advection in the soil it was critical to ensure that flow into and out of the probe were matched such that the sum of the probe  
163 and dilution flows were equal to the total flow at the instrument intake. This depended on precise flow control by digital mass  
164 flow controllers (MFC, Alicat Scientific, Tucson, AZ, USA). Dilution flow (Fig. 2) was important to reduce risk of  
165 condensation, avoid exceeding optimal detection range, and increase gas analyzer cell response time. The control gas system  
166 allowed us to stipulate the specific mole fractions and relative isotope mixtures at the column inlet. Two streams of UZA  
167 controlled by MFCs (probe and dilution) were delivered in tandem through a stream selector 16x2 port valve (VICI Valco

168 Instruments Inc. Houston, TX, USA) with the total flow directed to the analyzer (Fig. 2) by a second stream multipoint selector  
 169 (VICI Valco Instruments Inc. Houston, TX, USA). The custom control gas composition added to soil columns was mixed from  
 170 UZA and concentrated gas cylinders (e.g. 5% CO<sub>2</sub>; Table 3). A bypass line was installed to independently verify the control  
 171 gas composition entering the column while the column outflow line was used to measure column headspace concentrations  
 172 (Fig. 2). In System 1, we used a custom LabVIEW (National Instruments, Austin, TX) program to execute scripts generated  
 173 in Matlab (The MathWorks Inc.; 2018. Natick, Massachusetts) for timing and control of MFC gas flow rates and VICI valve  
 174 switching. The LabVIEW program queried and logged MFC parameters and SDI-12 via USB multi-drop box (BB9-RS232,  
 175 Alicat Scientific, Tucson, AZ, USA) interfaces. In System 2, TDLWintel, the TILDAS measurement and data acquisition  
 176 program, controlled the multi-valves on a schedule for continuous unattended operation.



177  
 178 **Figure 2.** Detailed schematic of sampling System 1 (UA) and System 2 (ARI). Column matrix gas concentrations were  
 179 controlled by mixing cylinder gas with UZA using MFCs and delivering the custom gas mixture through the columns from  
 180 bottom to top (orange dotted line). Probe sampling flow rates were controlled precisely using three MFCs to ensure that flow  
 181 in and out of the probe was balanced (*probe flow* (blue lines) + *dilution flow* (red lines) = *total flow to analyzer* (black lines)).  
 182 Column headspace (atmospheric pressure) and control gas bypass (positive pressure) were controlled by MFCs at two points  
 183 (*dilution*, *total flow to analyzer*), forcing the *probe flow* as a makeup flow (*probe flow* = *total flow* – *dilution flow*).

184 **Table 2.** Contrasting features between Systems 1 and 2

Feature	System 1	System 2
Objective	Feasibility of probe-TILDAS integration	Versatility of soil gas probe sampling
Location	University of Arizona, Biosphere 2, Tucson, AZ	Aerodyne Research Inc., Billerica, MA
Analyzer 1	Dual-laser TILDAS for H <sub>2</sub> O and CO <sub>2</sub> isotopes	Novel dual-laser TILDAS for N <sub>2</sub> O and CH <sub>4</sub> isotopes
Analyzer 2	Mini TILDAS for OCS, CO, CO <sub>2</sub> , and H <sub>2</sub> O	Vocus PTR-TOF-MS for VOCs
Control Gas (bulk)	Ultra-Zero Air	Ultra-Zero Air; Ultra-High Purity N <sub>2</sub>
Control Gas (trace)	5% CO <sub>2</sub> in air	49.1 ppm N <sub>2</sub> O in air; 54.6 ppm CH <sub>4</sub> in air
Flow Control	0.6 to 1 SLPM per column	0.65 SLPM per column
Matrix	Silica	Silica, Soil

185

186 To evaluate the probe and the column performance, we corrected observed concentrations ( $C_{obs}$ ) using the ratio of the  
 187 dilution and total flows to obtain true probe sample, column/headspace, and control gas concentrations ( $C$ ). For example, for  
 188 soil probe sample concentrations we used the ratio of the total flow ( $F_t$ ; probe plus dilution flow) to the probe flow ( $F_p$ ) as  
 189 shown in Equation 1:

190 
$$C = C_{obs} * F_t / F_p \tag{1}$$

191 **2.2 Trace gas analyzers**

192 We used a suite of trace gas analyzers relevant to biological soil gas cycling (Fig. 2) to integrate with the soil probe  
 193 sampling system. TILDAS isotope analyzers measure the concentrations of individual isotopologues, and isotopic ratios can  
 194 be determined using Equation (2):

195  
 196 
$$\delta^i X = (R_n / R_{reference} - 1) \times 1000$$
  
 197 
$$\tag{2}$$

198

199 where,  $R_n$  refers to the ratio of the rare isotopomer,  $^iX$ , to its abundant isotopomer (Toyoda et al., 2017).

## 200 2.2.1 Coupled laser spectrometers for CO<sub>2</sub> and H<sub>2</sub>O isotopes and COS and CO

201 In System 1 we integrated two TILDAS trace gas analyzers (Aerodyne Research, Inc., Billerica, MA, USA) with the  
202 soil probe system to evaluate the feasibility of coupling with the sintered PTFE probes and evaluate performance under  
203 controlled conditions. TILDAS-1 was a dual-laser instrument configured for measurement of water isotopes at 3765 cm<sup>-1</sup> and  
204 <sup>12</sup>C<sup>16</sup>O<sup>16</sup>O, <sup>13</sup>C<sup>16</sup>O<sup>16</sup>O, <sup>12</sup>C<sup>16</sup>O<sup>17</sup>O, <sup>12</sup>C<sup>16</sup>O<sup>18</sup>O O at 2310 cm<sup>-1</sup> with a 18 m absorption cell. TILDAS-2 was a compact ‘mini’  
205 single-laser instrument configured to quantify carbonyl sulfide (OCS), carbon monoxide (CO), water (H<sub>2</sub>O), and CO<sub>2</sub> at  
206 2050.4–2051.3 cm<sup>-1</sup> with a 76 m absorption cell. The dual and mini TILDAS analyzers had a 500 cm<sup>3</sup> and 300 cm<sup>3</sup> sample cell  
207 volume, respectively. The TILDAS platforms draw air samples through an absorption cell at low pressure where laser light is  
208 transmitted in a multi-pass configuration for long effective absorption path lengths. The laser is scanned at kilohertz rates over  
209 the rovibrational absorptions of the molecule(s) of interest. Transient light absorptions were fit to known Voigt profiles to  
210 determine molecular concentrations on-the-fly using Aerodyne’s proprietary acquisition and analysis software, TDLWintel.  
211 For this experiment we connected the two TILDAS analyzers at controlled flow rate (500–250 sccm, MC-1SLPM-D, Alicat)  
212 in series, and cell pressure was dynamically controlled to 40 Torr (PCSC-EXTSEN-D-15C/5P, Alicat) between the two  
213 analyzer sample cells and vacuum pump (MPU2134-N920-2.08, KNF Neuberger, Trenton, NJ). The TILDAS optical tables  
214 were each purged with 100 sccm zero air.

215 In System 1, CO<sub>2</sub> concentrations varied linearly with controlled dilutions of 10% CO<sub>2</sub> tanks (Fig. S1 dual CO<sub>2</sub> cal),  
216 and absolute CO<sub>2</sub> concentrations were calibrated with a linear curve. We calibrated the  $\delta^{13}\text{C-CO}_2$  from the concentration  
217 dependent relationship of  $\delta^{13}\text{C-CO}_2$  vs observed [CO<sub>2</sub>] (Fig. S2); specifically, we fit a gaussian equation to the relationship  
218 between ( $\delta^{13}\text{C-CO}_2^{\text{observed}} - \delta^{13}\text{C-CO}_2^{\text{true}} \sim -39.2 \text{ ‰}$  vs Vienna PeeDee Belemnite (VPDB)) and CO<sub>2</sub> concentration (accounting  
219 for standard deviation in  $\delta^{13}\text{C-CO}_2$  measurements). We applied this CO<sub>2</sub>-dependent correction to all reported  $\delta^{13}\text{C-CO}_2$  values.

## 220 2.2.2 Novel laser spectrometer for N<sub>2</sub>O and CH<sub>4</sub> isotopomers

221 System 2 integrated a second and nearly identical (Table 2) gas sampling system with a novel dual TILDAS analyzer  
222 for isotopomers of methane (CH<sub>4</sub>) and nitrous oxide (N<sub>2</sub>O) (Aerodyne Research, Inc., Billerica, MA, USA) to test instrument  
223 modifications that help integrate soil gas sampling probes with laser spectrometry.

224 In this study, we identified and selected the best spectral region and laser technology for continuous high precision  
225 measurements of isotopomers of CH<sub>4</sub> (<sup>12</sup>CH<sub>4</sub> and <sup>13</sup>CH<sub>4</sub>), and N<sub>2</sub>O (<sup>14</sup>N<sup>14</sup>N<sup>16</sup>O (“446”), <sup>14</sup>N<sup>15</sup>N<sup>16</sup>O (“456”), <sup>15</sup>N<sup>14</sup>N<sup>16</sup>O (“546”),  
226 and <sup>14</sup>N<sup>14</sup>N<sup>18</sup>O (“448”). The regions near 2196 cm<sup>-1</sup> (4.56 μm) and 1295 cm<sup>-1</sup> (7.72 μm) provide interference-free  
227 measurements of N<sub>2</sub>O and CH<sub>4</sub>, respectively, and their rare isotopes. The 2196 cm<sup>-1</sup> region is also capable of measuring CO<sub>2</sub>  
228 at soil-relevant concentrations (parts-per-thousand levels). The CH<sub>4</sub> and N<sub>2</sub>O TILDAS system was optimized with respect to  
229 optical alignment, laser operating parameters (i.e., scan length, laser current and temperature settings), and fit parameters.

230 Short- (seconds) and long-term (minutes-hours) noise were determined by sampling from a compressed air cylinder as a  
231 constant gas source, followed by Allan-Werle variance analysis (Werle et al., 1993). We chose 30 Torr as the optimum cell  
232 pressure to minimize both noise and spectral crosstalk between isotopomer absorptions. To reduce sample volume we designed  
233 a new cell insert and a compact 76 m pathlength multipass sampling cell. The novel volume-reducing insert for the 76 m cell  
234 has interior walls that match the contour of the multipass pattern and was 3D-printed using PA2200 nylon. After printing, the  
235 interior and exterior surfaces of the insert were sealed with urushi lacquer—a stable, durable, inert lacquer (McSharry et al.,  
236 2007). The turnover time of the cell volume with insert was evaluated in continuous sampling mode.

237 The concentration dependence of isotope  $\delta$  values derived from infrared isotopic measurements is an analytical  
238 challenge that is instrument dependent. To minimize the concentration dependence we used: (i) frequent spectral backgrounds  
239 to minimize offsets (i.e., immediately prior to each sample measurement), A sample spectrum is recorded with the instrument  
240 sample cell filled with UZA. This spectrum is used to normalize sample spectra, improving accuracy and sensitivity by  
241 accounting for changing instrument conditions and possible drift; and (ii) identified best fitting parameters for each spectral  
242 region and application. During System 2 operation, we automated script schedules using an external command language (ECL)  
243 within TDLWintel that ran backgrounds, calibrations, and controlled valves.

244 Alcohols (e.g. methanol and ethanol) have weak features in the methane spectral window ( $1295\text{ cm}^{-1}$ ), at levels  
245 typically below that of the isotopic precision. We tested whether VOCs would cause infrared spectral interferences with  
246 TILDAS analysis by exposing the instrument to artificially elevated part-per-thousand levels of methanol, ethanol, and  
247 formaldehyde—three species that may be common in soil. We found potential for interference near the  $^{13}\text{CH}_4$  absorption at  
248 elevated alcohol levels, but did not observe this interference in the spectra collected from probes in the soil tested.

249 System 2 calibration used online mass flow control to dilute concentrated  $\text{N}_2\text{O}$  or  $\text{CH}_4$  calibration gases into UZA.  
250 We used pure samples of  $\text{N}_2\text{O}$  from Massachusetts Institute of Technology (MIT Ref I and Ref II). The isotopic ratios of  $\text{N}_2\text{O}$   
251 were determined by Isotope Ratio Mass Spectrometry (IRMS) and TILDAS measurements, and externally verified by *S.*  
252 *Toyoda* at Tokyo Institute of Technology (McClellan, 2018). For calibration of the soil matrix tests discussed below, we used  
253 MIT Ref II to make a surveillance standard of 1,000 ppm  $\text{N}_2\text{O}$ . After calibrating  $\text{N}_2\text{O}$  isotopes against the reference gas,  
254 observed lab air  $\text{N}_2\text{O}$  isotopic ratios were within 3‰ of the relatively stable isotopic ratios of ambient tropospheric  $\text{N}_2\text{O}$  (Snider  
255 et al., 2015): bulk  $^{15}\text{N}$  value of 6.3-6.7‰, and site preference of 18.7‰ (Mohn et al., 2014), and  $^{18}\text{O}$  value of 44.4‰ (Snider  
256 et al., 2015). For  $\text{CH}_4$  concentrations, a  $\text{CH}_4$  surveillance tank served as a stable isotopic source to identify changes in isotopic  
257 composition. Measured instrumental precisions were 0.9‰ and 1.6‰ for  $\text{N}_2\text{O}$  bulk  $^{15}\text{N}$  and site preference, and 0.2‰ for  
258  $^{13}\text{CH}_4$ .

259

## 260 2.2.3 High resolution volatile organic compound gas analyzer

261 In System 2 experiments, we integrated a PTR-TOF-MS (Vocus; Aerodyne Research Inc., Billerica, MA, USA)  
262 (Krechmer et al., 2018) into the sampling system in parallel with the N<sub>2</sub>O/CH<sub>4</sub> TILDAS, to detect soil VOCs such as  
263 monoterpenes, isoprene, and pyruvic acid (Gonzalez-Meler et al., 2014; Guenther et al., 1995). The Vocus technology contains  
264 a corona discharge reagent-ion source and focusing ion molecule reactor (fIMR) that has low limits of detection (less than part  
265 per trillion by volume) and fast time response, acquiring the entire mass-to-charge spectrum on the order of microseconds. A  
266 TOF instrument also has high resolving power in the mass dimension, enabling separation of isobaric signals (occurring at the  
267 same nominal mass-to-charge ratio). The TOF employed in this work consisted of a 1.2 m flight tube enabling a resolving  
268 power > 10,000 m/Δm. A sample flow of 100 SCCM was injected continuously into the Vocus source, with no extra overblow  
269 or carrier flow in the inlet line.

270 Data was processed using the Tofware (Aerodyne/TOFWERK A.G.) software package in Igor Pro (Wavemetrics).  
271 For these experiments PTR-TOF-MS was not quantitatively calibrated for the signals reported below, as we were only  
272 interested in relative concentration responses to wetting. Thus, signals are reported in non-normalized counts/s (Hz).

## 273 2.3 Experiments performed

274 We performed experiments using Systems 1 and 2 (Section 2.2; Fig. 2) to demonstrate the feasibility and versatility  
275 in coupling the permeable soil gas probes to trace gas analyzers to measure in situ gas concentrations and isotope ratios in  
276 soils. We conducted two categories of experiments: 1) *Experiments under controlled conditions using silica*, characterizing  
277 the ability of probe sampling to measure known, controlled soil gas concentrations; and 2) *Experiments with soil*, characterizing  
278 the ability of probes to capture soil microbial gas cycling dynamics from natural soils in response to environmental changes.

### 279 2.3.1 Experiments under controlled conditions using silica

280 Silica sand was used to limit trace gas production or consumption from the matrix for controlled evaluation of the  
281 probe. Three columns were filled with a dry silica matrix (Table S1) and closed hermetically. Gas concentrations and isotopic  
282 signatures of the inlet, soil probe, and column headspace samples were quantified while the gases flowed continuously through  
283 the column and dilutions rates were varied (Table 3).

284 We evaluated the *effect of probe sampling on the column* (Experiment 1) by changing the probe flow rate with constant  
285 control gas concentration and dilution. With System 1 and a single column, we alternated measurement of CO<sub>2</sub> concentration  
286 in headspace gas (1 h) and the probe (15 min) to determine the impact of probe sampling on soil column outflow concentrations.  
287 Next, we tested the flow conditions that support the probe delivering fully equilibrated and representative samples by *varying*  
288 *flow and dilution* at constant column concentrations (Experiment 2). We evaluated 42 combinations of set points for total flow

289 (from 50 to 300 sccm, at 50 sccm intervals) and dilution (from 90% to 9%, at 15% intervals). Each measurement cycle lasted  
 290 25 min (15 min probe; 10 min column headspace) using one probe in System 1 and System 2.

291 We scaled-up the sampling systems to three probes to evaluate multiple probes (Experiment 3). We measured probe  
 292 and headspace gas at a constant dilution (75%) of a 2000 ppm CO<sub>2</sub> control gas for a target observation concentration of 500  
 293 ppm and probe flow rates of 5, 10, 20, 30, 40, 50, and 100 sccm (System 1). System 2 was similarly evaluated with N<sub>2</sub>O and  
 294 CH<sub>4</sub> control gases in the silica matrix (Table 3).

295 **Table 3.** Experiments under controlled conditions with silica matrix using Systems 1 and 2

Experiment	Columns	Probe Pore Size (µm)	Total flow (sccm); Probe Flow (sccm); Dilution (%)	Control gas (ppm)	System
1. Effect of probe sampling (silica) <sup>a</sup>	1	P8 (8 µm)	total (10-600); probe (5-300); dilution (50%)	CO <sub>2</sub> 1000	1
2. Flow and dilution <sup>a</sup>	1	P8 (8 µm)	total (50:50:300); probe (0-300); dilution (90:15:0%)	CO <sub>2</sub> 1000	1, 2
3. Multi-probe evaluation <sup>a</sup>	1	P8 (8 µm)	total (20-400); probe (5-100); dilution (75%)	CO <sub>2</sub> 2000	1
	2	P10 (10 µm)			
	3	P5 (5 µm)			
	4	P8 (8 µm)	total (250); probe (25); dilution (90%)	N <sub>2</sub> O 3ppm CH <sub>4</sub> 7 ppm	2
	5	P10 (10 µm)			

296 <sup>a</sup>Experiments 1-3 were conducted with the column top closed and no water addition.

### 297 2.3.2 Experiments with soil

298 We replaced the silica matrix with soil in the columns to understand (1) probe behavior and response when monitoring  
 299 soil gases in a complex and dynamic soil matrix and (2) soil processes that drive dynamic changes in subsurface soil gases.  
 300 We measured N<sub>2</sub>O and CH<sub>4</sub> concentrations and isotopic signatures with the improved TILDAS instrument on System 2 (Fig.  
 301 2) in a series of experiments (Table 4). For soil experiments, headspace measurements can be used to track surface gas fluxes,  
 302 but do not represent control gas concentrations as in the silica experiments. We evaluated how measured soil gas concentrations  
 303 changed in response to: probe sample flow rate (Experiment 4); environmental manipulations to the soil matrix (e.g. increased  
 304 soil moisture with 5.1 cm of simulated rainfall) (Experiment 5); and forced changes to soil redox state (e.g. forced N<sub>2</sub> and UZA  
 305 through the columns to shift from anoxic to oxic soil environments) (Experiment 6). In this last experiment, we integrated the  
 306 Vocus PTR-TOF-MS to the system to measure soil VOCs (Fig. 2).

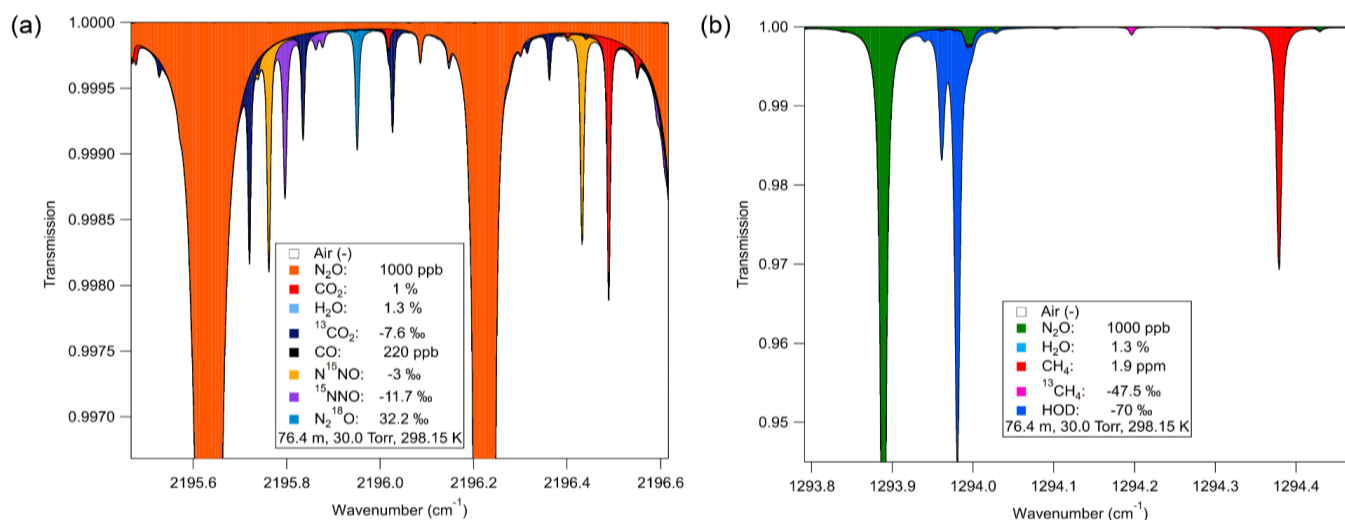
Experiment	Type of soil	Columns	Probe	Total flow (sccm); Probe Flow (sccm); Dilution (%)	Control Gas/Flush	Soil Moisture
4. Soil vs. silica: multi-probe flow rate dependence	Soil 1	4	P8 (8 um)	total (235); probe (60); dilution (74%)	Capped <sup>c</sup>	Field moisture
	Silica	5	P10 (10 um)		N <sub>2</sub> O 3 ppm; CH <sub>4</sub> 7 ppm	Dry
	Silica	6	P25 (25 um)			Dry
5. Soil wetting <sup>a</sup>	Soil 1	4	P8 (8 um)	total (50-100); probe (25); dilution (50-75%)	NA <sup>d</sup>	Dry to wet
6. Soil redox: anoxic (N <sub>2</sub> ) to oxic (UZA) <sup>ab</sup>	Soil 3	5	P10 (10 um)	total (185); probe (53); dilution (71%)	UZA <sup>e</sup>	Wet

308 <sup>a</sup> Experiment conducted with the column top open.309 <sup>b</sup> Experiment integrated Vocus PTR-TOF-MS for VOCs.310 <sup>c</sup> Measurements performed with the column closed.311 <sup>d</sup> Not applicable (NA), control gas was not used during the experiment.312 <sup>e</sup> Matrix flushed with Ultra Zero Air (UZA) on a capped (close) column to change condition only.313 **2.4 Data processing**

314 For System 1, we used RStudio and R version 3.3.2 (Team, 2017) to integrate raw with metadata. Igor Pro (version  
315 7, WaveMetrics, Lake Oswego, OR) for System 1 and System 2 was used to analyze instrument diagnostic, concentrations  
316 and times series. We averaged the last 80% to 90% of each measurement. Measurements were dilution corrected to obtain  
317 undiluted sample concentrations (Equation 1). In controlled tests when true headspace concentrations were measured before  
318 and after a probe measurement, these values were interpolated for comparison against probe concentrations to determine  
319 fractional recovery of soil gas concentrations.

320 **3. Results**321 **3.1 Instrument improvement (N<sub>2</sub>O/CH<sub>4</sub> isotopomer TILDAS)**322 **3.1.1 Selection of spectral regions**

323 We selected optimal spectra windows and laser technologies for detection of the isotopomers of both CH<sub>4</sub> and N<sub>2</sub>O  
 324 using fundamental rovibrational transitions (Fig. 3). We used Aerodyne-developed simulation programs that utilize the  
 325 HITRAN database (Rothman et al., 2013) to perform spectral simulations to identify potential measurement regions. Based on  
 326 these simulations, we obtained appropriate lasers and detectors for the selected spectral regions. Simulations assumed an N<sub>2</sub>O  
 327 mixing ratio of 1 ppm (parts per million, lower end of expected (Rock et al., 2007) in a mixture with 1.3% H<sub>2</sub>O, 1% CO<sub>2</sub>, 220  
 328 ppb CO and 1.9 ppm CH<sub>4</sub>, at 30 Torr in a 76.4 m pathlength sample cell. This resulted in the selection of a spectral region  
 329 (Fig. 3a) where all four N<sub>2</sub>O isotopomers of interest, <sup>14</sup>N<sup>14</sup>N<sup>16</sup>O (“446”), <sup>14</sup>N<sup>15</sup>N<sup>16</sup>O (“456”), <sup>15</sup>N<sup>14</sup>N<sup>16</sup>O (“546”), and <sup>14</sup>N<sup>14</sup>N<sup>18</sup>O  
 330 (“448”), have absorptions in close spectral proximity (<1 cm<sup>-1</sup>), but without overlap of absorptions of each other or other trace  
 331 gases such as from CO<sub>2</sub>. The 2196 cm<sup>-1</sup> region was used to monitor the N<sub>2</sub>O isotopologues and CO<sub>2</sub> in the soil gas matrix using  
 332 a quantum cascade laser (QCL) (Alpes Laser, Switzerland). We selected a second QCL (Alpes Laser) based on simulations of  
 333 methane isotopes in the 1294 cm<sup>-1</sup> region to monitor <sup>12</sup>CH<sub>4</sub> and <sup>13</sup>CH<sub>4</sub> isotopomers (Fig. 3b). This region also provided  
 334 measurement of H<sub>2</sub>O content in the soil gas via a water spectral feature at ~1294.0 cm<sup>-1</sup>.



335 **Figure 3.** Isotopomers spectral regions for monitoring N<sub>2</sub>O and CH<sub>4</sub> isotopomers. (a) N<sub>2</sub>O isotopologue spectrum near 2196  
 336 cm<sup>-1</sup>. Four N<sub>2</sub>O isotopomers were present and spectrally separated, yellow and purple refer to the <sup>15</sup>N isotopomers with  
 337 different positions relative to the oxygen. Blue refers to the <sup>18</sup>O isotopomer. (b) Spectral simulation of 1294 cm<sup>-1</sup> region for  
 338 methane analysis with lines well separated from H<sub>2</sub>O and N<sub>2</sub>O.

### 339 3.1.2 Optimization of isotope ratio measurements

340 TILDAS operational parameters were optimized to increase isotope ratio precision. For example, we monitored the  
 341 slightly weaker doublet at 2196.2 cm<sup>-1</sup> that had lower concentration dependence than the stronger absorber singlet at 2195.6

342 cm<sup>-1</sup> that would produce nonlinear dependence at high mixing ratios. In addition, we modified fitting parameters to minimize  
343 impact of baseline variability on measurement precision (fit shown in Fig. S3). These improvements in spectral fitting helped  
344 minimize the dependency of N<sub>2</sub>O and CH<sub>4</sub> isotopic ratios on concentration. Specifically, we reduced the slope of  $\delta$  vs mole  
345 fraction to 0.7 ‰ ppm<sup>-1</sup> N<sub>2</sub>O (for N<sub>2</sub>O < 8 ppm) and 0.5 ‰ ppm<sup>-1</sup> CH<sub>4</sub> (for CH<sub>4</sub> < 14 ppm). The online dilution approach was  
346 critical for avoiding N<sub>2</sub>O and CH<sub>4</sub> concentrations in soil exceeding these linear ranges. We quantified the precision of the  
347 isotopic ratios (Table S2) using Allan-Werle plots (Werle et al., 1993) (Fig. S3).

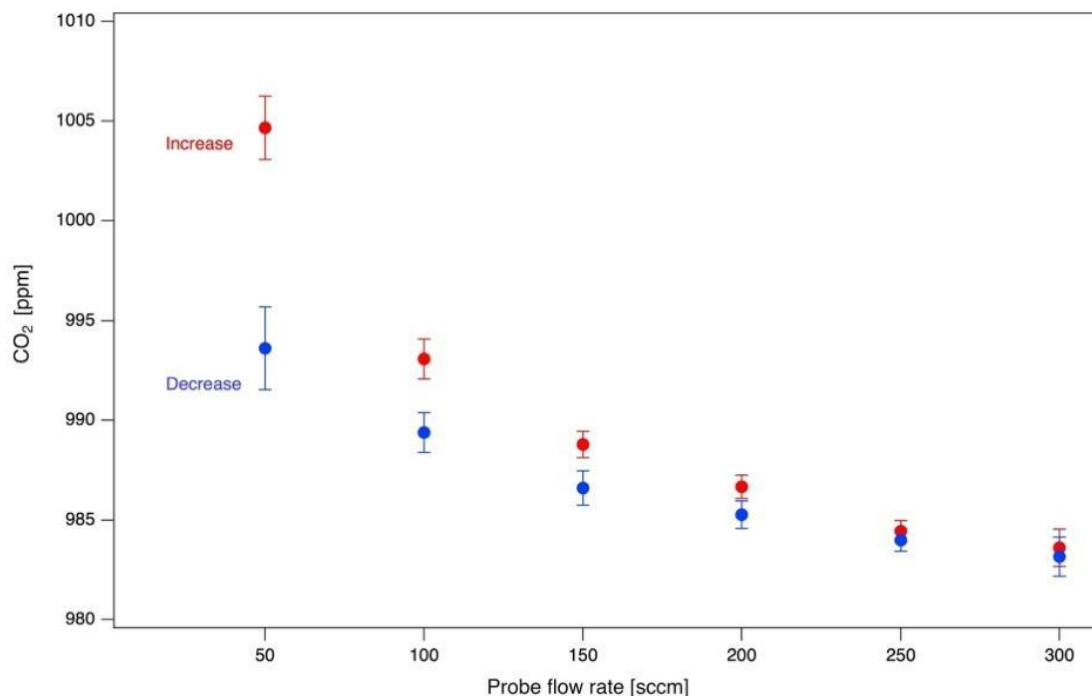
### 348 **3.1.3 Sample cell reduction**

349 We improved measurement response time by reducing TILDAS sample cell volume while maintaining the  
350 spectroscopic path length. Unnecessary ‘dead’ volume in the sample cell was eliminated through two approaches. First, we  
351 reduced the cell volume (port to port) by 20% (610 cm<sup>3</sup> to 485 cm<sup>3</sup>) by shortening the cell by 4.2 cm, eliminating dead volume  
352 behind the mirrors. Second, the insert reduced the cell volume by ~50% (485 to 245 cm<sup>3</sup>) by filling volume between the  
353 mirrors, but in the region outside of the multi-pass laser path. Overall, these changes reduced cell volume from 610 cm<sup>3</sup>  
354 (previous ARI 76-m Astigmatic Multipass Absorption Cell (AMAC) cell) to 245 cm<sup>3</sup>, which improved the cell response time  
355 by 40%, here defined as the time to observe 75% of a full transition in concentration (Fig. S4) (i.e. from 1.13 (0.005) s to 0.76  
356 (0.01) s; 30 Torr and 1 SLPM). At the cell pressure of 30 Torr used here, this 245 cm<sup>3</sup> absorption cell volume corresponds to  
357 9.7 cm<sup>3</sup> of sample gas at ambient pressure.

## 358 **3.2 Probe integration with gas sampling system: performance and optimization**

### 359 **3.2.1 Effect of probe sampling on soil gas concentrations (Experiment 1)**

360 Soil probes sample subsurface gases by diffusion across the probe membrane into a UZA stream flowing through the  
361 probe. In our balanced mass flow approach, an equal proportion of UZA molecules diffuse out of the probe relative to soil gas  
362 diffusing in, which can affect (i.e., dilute) concentrations in the subsurface environment. To quantify the impact of probe  
363 sampling on soil column concentrations, we set control gas to 1000 ppm CO<sub>2</sub> and varied the probe flow rate from 5 to 300  
364 sccm, and back, at a constant dilution (50%). We evaluated the impact of a 15-min soil probe measurement on subsequent 1-  
365 hour measurements of the column headspace. We found that column CO<sub>2</sub> concentrations were depleted directly following  
366 probe sampling (from 0.6 to 1.6% depletion) and took > 1 hour to fully stabilize. Column CO<sub>2</sub> was most depleted after higher  
367 probe flow rates (Fig. 4) due to increased CO<sub>2</sub>-free UZA diffusion through the probe membrane. Low probe flow rates helped  
368 minimize these sampling artifacts on subsurface concentrations.

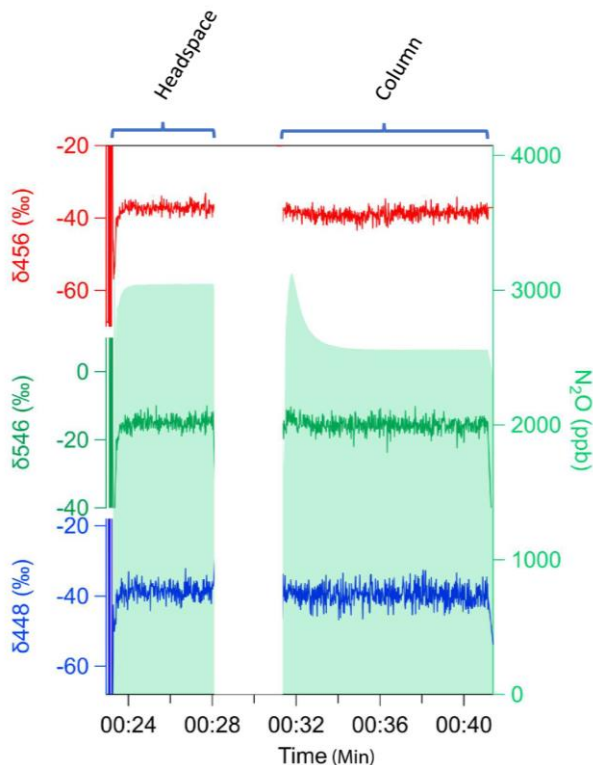


369 **Figure 4.** Effect of probe flow rate on column gas concentration (System 1), representing the potential impact of probe  
 370 sampling on the soil environment. Points represent concentration of CO<sub>2</sub> in the headspace column for one hour after a 15-min  
 371 probe sampling event at various increasing (forward) and decreasing (reverse) probe sampling flow rates.

### 372 3.2.2 Impact of probe flow rate and dilution on residence time of gas in probes, (Experiment 2)

373 Compared to the controlled soil gas concentrations (Fig. 5), the probe-sampled concentrations were lower. When  
 374 probe carrier gas is not flowing, the volume inside the probe is fully equilibrated with soil gas. This resulted in the observed  
 375 initial ‘pulse’ of high gas concentrations when a probe was first selected and measured. During sampling, probe gas  
 376 concentrations drop to a steady-state value that represents a balance between probe flow rate and the diffusion rate of soil gas  
 377 molecules into the probe.

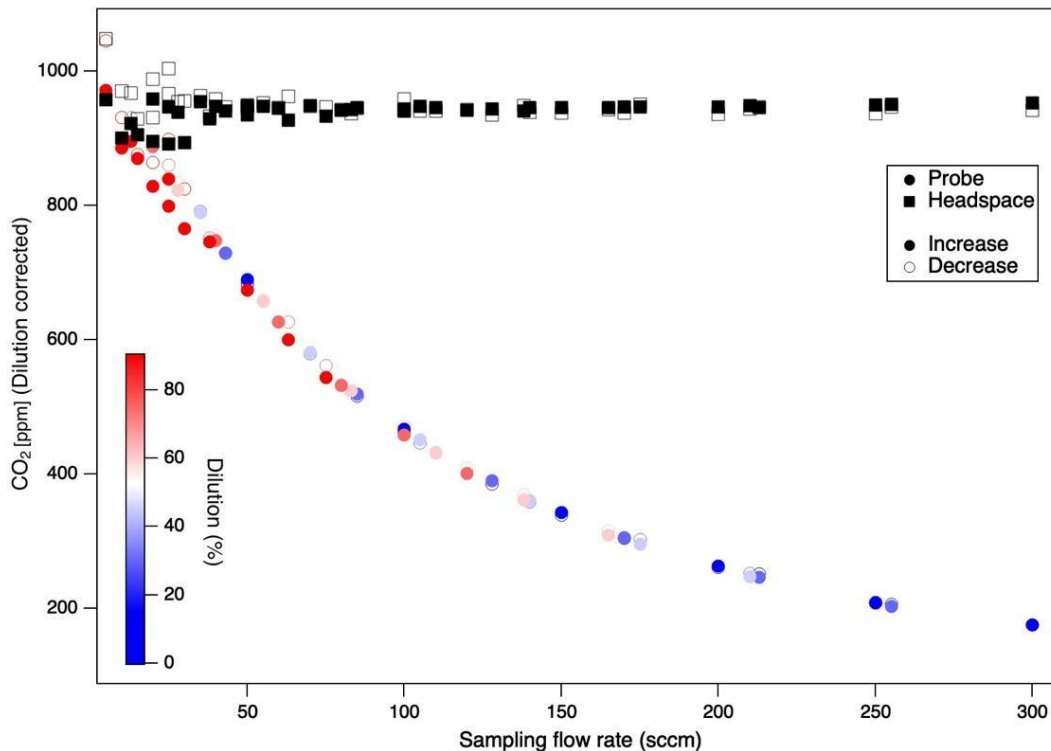
378



379

380 **Figure 5.** Headspace and probe measurements of N<sub>2</sub>O using silica in System 2 (CH<sub>4</sub>/N<sub>2</sub>O). Example of initial pulse that  
 381 equilibrates under flow-through and incomplete diffusion of N<sub>2</sub>O concentration (green shade) with undetectable isotopic  
 382 fractionation of isotopomers δ456 (red), δ546 (green), δ448 (blue).

383 Gas samples obtained by probes at low probe flow rates were most representative of soil gas, as the slower flow rates  
 384 allow more complete diffusive equilibration. We evaluated the impact of combinations of different total flow rates (from 50  
 385 to 300 sccm at 50 sccm increments) with sample dilution ratios (from 0 to 90% dilution at 15% increments) resulting in probe  
 386 sampling flow rates between 5 and 300 sccm. These tests were conducted in the silica matrix with controlled soil gas  
 387 composition (1000 ppm CO<sub>2</sub>) (Experiment 2). We calculated the residence time of carrier gas in the soil probe by considering  
 388 the internal volume of the probes (V=2.6-4.6 mL) and the range of flow rates evaluated (F=5-300 sccm). This indicates that  
 389 the residence time (V/F) could range from <1 sec for high flow rates to 55 sec for the lowest flow rates and larger volume (5  
 390 sccm in probes P5, P8, P10). We found that observed soil probe concentrations decreased with increases in probe flow rate  
 391 (Fig. 6, Fig. 7), with no systematic influence of the dilution ratio. For the probe tested (Table 4), flow rates below 24.5 sccm  
 392 produced representative samples (within 90% of true concentration). We did not observe any clear drawbacks to sampling CO<sub>2</sub>  
 393 at flow rates <50 sccm (Fig. 7).

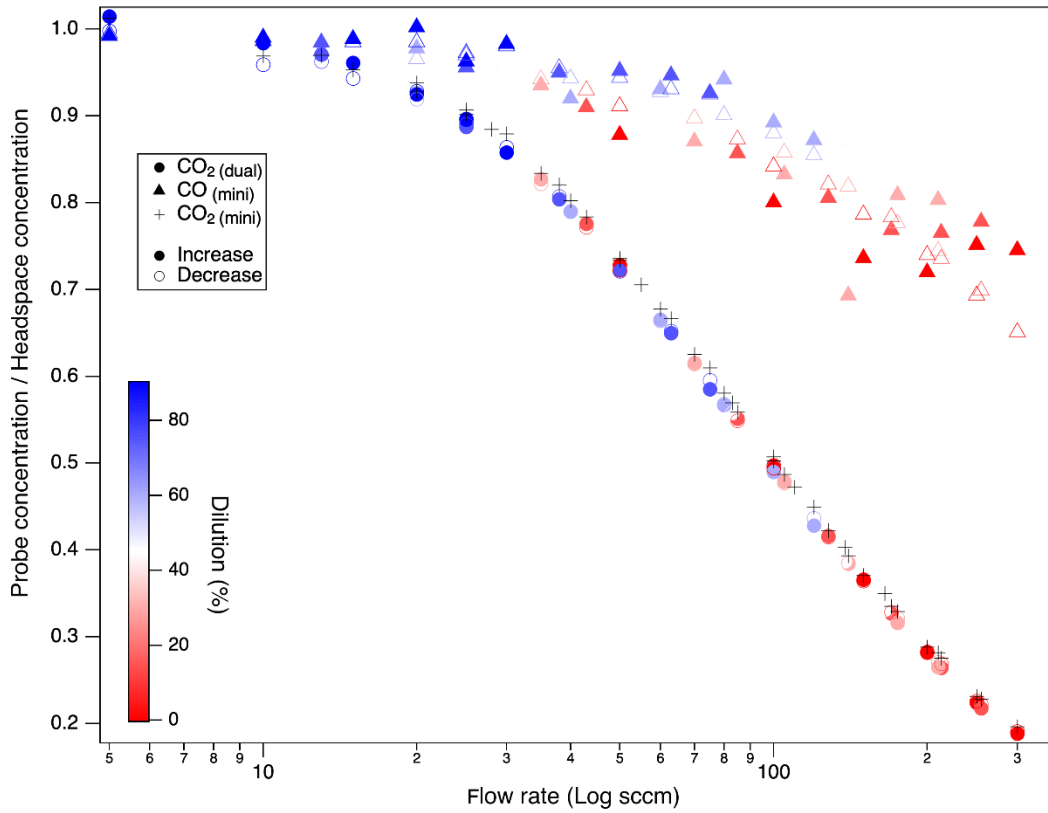


394 **Figure 6.** Probe and headspace CO<sub>2</sub> over a range of probe flow rates and dilution ratios (color), reflecting the  
 395 recovered sample vs. true gas concentrations, respectively. Column soil gas concentrations (headspace) remained steady across  
 396 the experiment, while gas concentrations sampled by the probe diverged from true values at high probe sampling flow rates.  
 397 Similar patterns were observed for independent experiments run with the reverse sequence from low to high vs. high to low  
 398 probe flow rates (open vs closed symbols). CO<sub>2</sub> concentrations are dilution corrected (System 1 Dual).

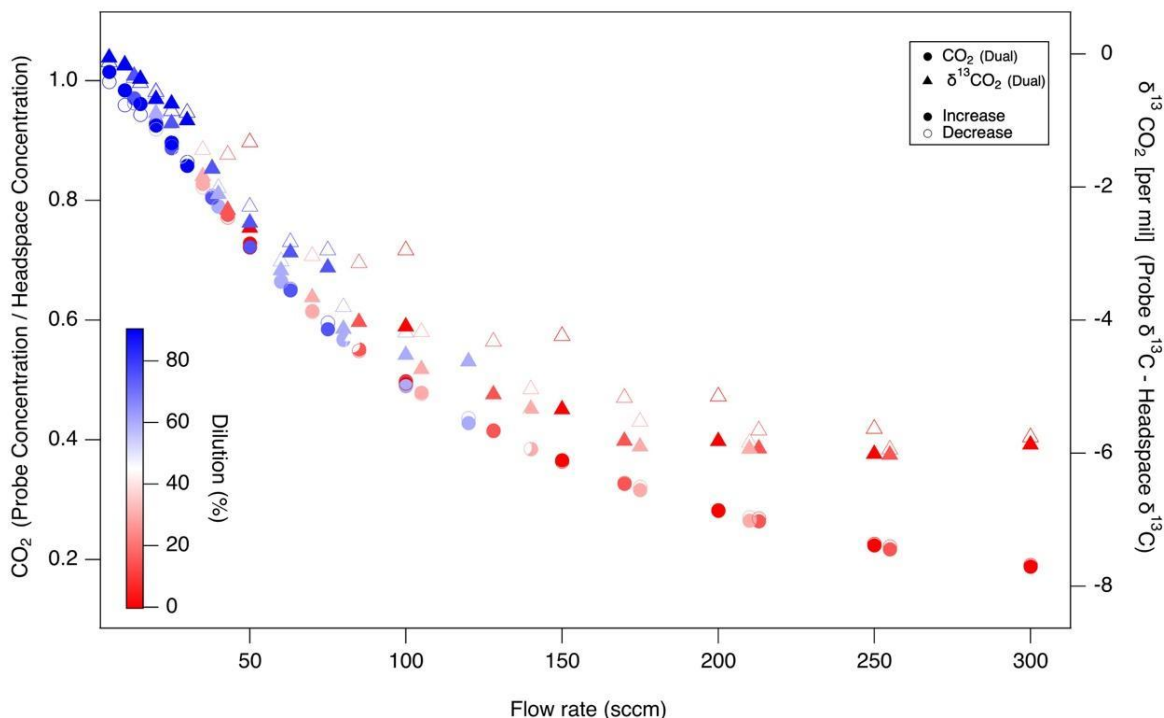
399 Probe flow rates affected gases unequally, and based on their diffusivity. Probe recovery was lower for CO<sub>2</sub> with  
 400 lower diffusivity than CO (molecular diffusion coefficients in air at 20°C: (CO<sub>2</sub> 0.14, CO 0.18) (Bzowski et al., 1990;  
 401 Massman, 1998) (Fig. 7). The fractional recovery of true soil gas concentrations by probe gas sampling (i.e., probe:column  
 402 headspace ratios) was higher (0.65) for CO than CO<sub>2</sub> (0.2) at high flow rates (300 sccm). Additionally, the recovery ratios at  
 403 specific flow rates were more scattered at a higher flow rate for CO. Regardless of the diffusion coefficient, both CO<sub>2</sub> and CO  
 404 reached equilibrium at low probe flow rates, but CO was well-equilibrated over a 4x wider range (5-100 sccm) than CO<sub>2</sub> (5-  
 405 25 sccm). Moreover, for molecular isotopologues (e.g., <sup>12</sup>CO<sub>2</sub> vs <sup>13</sup>CO<sub>2</sub>), at increasing probe flow rates, the sampled CO<sub>2</sub> δ<sup>13</sup>C  
 406 appears to be lighter than the headspace control by ~ -6 ‰ (Fig. 8) at the highest probe flow rates. That this fractionation was  
 407 observed relative to the headspace measurements implies it is derived from the probe, rather than the rest of the sampling  
 408 system (tubing, multiport valves, MFCs). These concentration and isotopic fractionation results underscore the need to ensure

409 that the probe flow rate is sufficiently low to ensure full diffusive exchange between zero air and soil gas before the gas sample  
410 exits the probe.

411



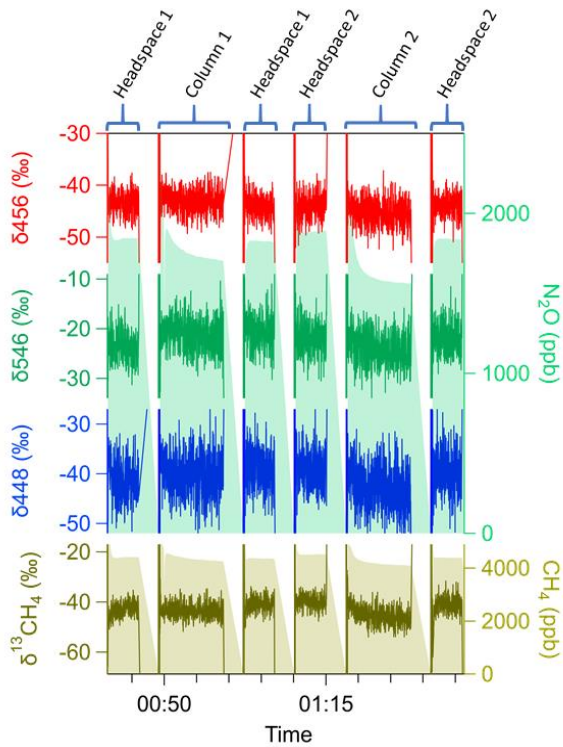
412 **Figure 7.** Impact of probe sampling flow rate on the fractional recovery of true gas concentrations by probe gas sampling for  
413 trace gases with differing diffusivity ( $\text{CO} > \text{CO}_2$ ) respectively, represented as the fractional recovery (probe:headspace  
414 concentration ratio) during a test with a sequential increase in probe flow rate (forward in filled symbols) followed by a test  
415 decreasing (reverse in open symbols) the flow rates. Dilution corrected  $\text{CO}_2$  and  $\text{CO}$  on System 1.



416 **Figure 8.** Impact of probe sampling flow rate on the fractional recovery of true CO<sub>2</sub> concentrations (left axis, circles) and the  
 417 offset in true soil δ<sup>13</sup>C (right axis, triangles) by probe gas sampling. As in Fig. 7, sequential probe flow rate increases (filled  
 418 symbols) and decreases (open symbols) tests plotted together. Dilution corrected in System 1.

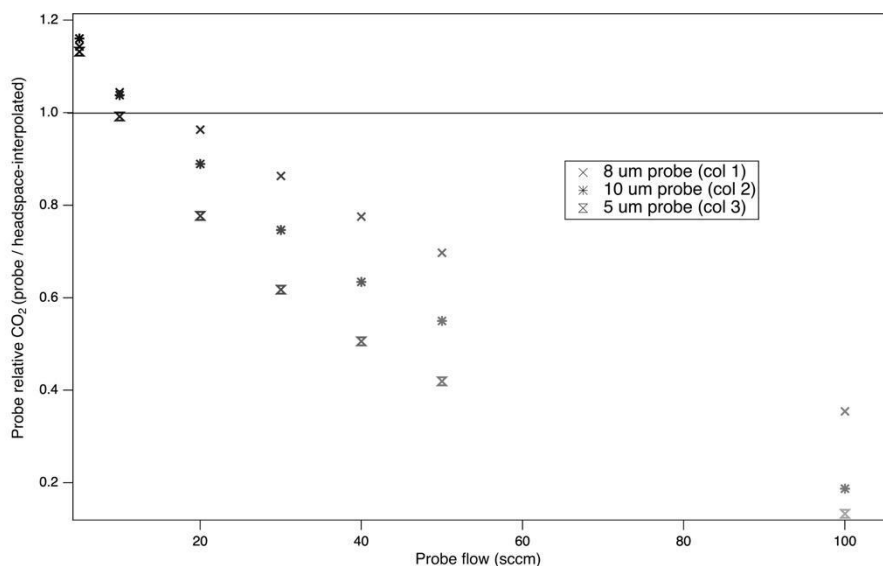
### 419 3.2.3 Demonstration with multiple probes (Experiment 3)

420 We up-scaled the online diffusive probe sampling method in both System 1 and 2 to automatically control multiple  
 421 probes using at flow rates (<100 sccm) to measure soil gas concentrations and isotopic ratios (Figure E). To fully constrain  
 422 probe measurements in the silica matrix (Table 3), each probe was evaluated repeatedly over a full sampling cycle (~25  
 423 minutes) to measure headspace-probe-headspace. In both systems, we could scale to sequential measurements of multiple  
 424 probes with good sample recovery (e.g., minimal concentration loss, isotope fractionation). In particular, probe recovery of  
 425 N<sub>2</sub>O isotopomers was within 3% from true headspace values, and equilibration of all trace gas species generally was near or  
 426 above 85% (Fig. 9). Multiprobe tests showed that the system has a high potential for scalable spatial resolution and scalability.  
 427



428 **Figure 9.** Soil probe sampling approach up-scaled to multiple probes (System 2). Multiprobe tests measured headspace-probe-  
 429 headspace sequentially for (top panels) N<sub>2</sub>O (green shade; right side) including isotopic ratios for three N<sub>2</sub>O isotopomers δ<sub>456</sub>  
 430 (red), δ<sub>546</sub> (green), δ<sub>448</sub> (blue) and (bottom panel) δ<sup>13</sup>C-CH<sub>4</sub> (brown; left axis) and CH<sub>4</sub> (brown shade; right axis) in the left  
 431 axis.

432 We used the multiprobe system to determine whether probes with different properties would exhibit the same flow  
 433 dependency, and in particular, the effect of characteristic pore size of a sPTFE probe on concentration recovery. The flow rate  
 434 dependence of the different probes was determined with CO<sub>2</sub> in silica sand (Fig. 10). We found that the flow rate dependency  
 435 for one pore size (P1) predicted the general behavior of others (P2-P3) across a 5-10 μm pore size range. Unexpectedly, we  
 436 did not find a clear link between the pore size and the fractional recovery of true soil CO<sub>2</sub> concentrations for any given flow  
 437 rate. For example, we might expect that a pore size of 10 μm would permit greater diffusion and favor probe equilibration;  
 438 instead, the 8 μm probe produced a more equilibrated sample than either the 5 μm or 10 μm (Fig. 10).



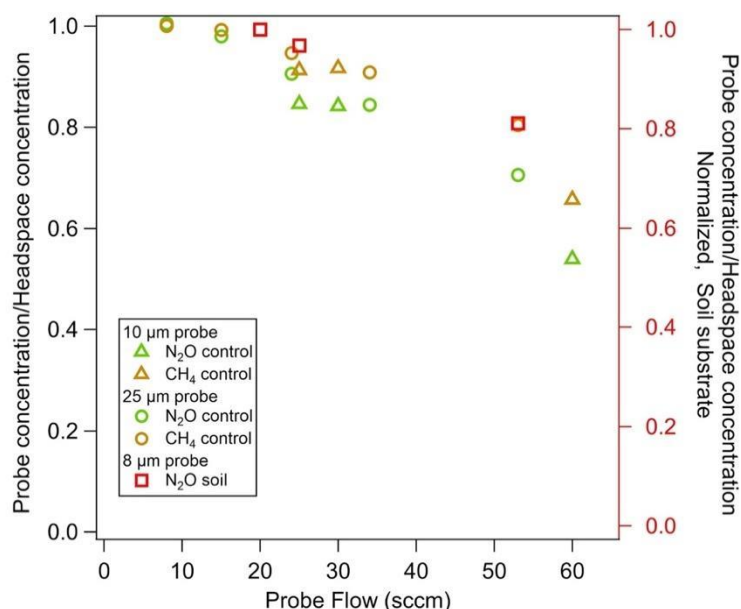
439 **Figure 10.** Impact of probe pore size on the relationship between probe sampling flow rate and fractional recovery of true soil  
 440 gas concentrations. Multiprobe test with System 1. Column headspace-probe-headspace were measured sequentially, and  
 441 headspace values were interpolated to calculate the fractional recovery.

#### 442 3.2.4 Comparison of probe flow rate dependency in soil vs silica (Experiment 3 and 4).

443 In System 2, at low probe flow rates the concentration measured from the probe was similar to the concentration in  
 444 the headspace in the silica matrix. Probe flow rates above 25 sccm decreased probe concentration for both the 10  $\mu\text{m}$  and 25  
 445  $\mu\text{m}$  pore sizes (Fig. 11). Similar to System 1 (Fig. 10), the fractional recovery did not increase with pore size, and we did not  
 446 find that the 25  $\mu\text{m}$  pore size transferred more gas into the carrier flow. In tests at higher probe flow in the silica matrix, the  
 447 fraction of  $\text{CH}_4$  recovered in the probe was higher than for  $\text{N}_2\text{O}$ , consistent with System 1 results (Fig. 7) and the known  
 448 molecular diffusion rates of  $\text{N}_2\text{O}$  and  $\text{CH}_4$  through soil,  $0.14 \text{ cm}^2 \text{ s}^{-1}$  and  $0.19 \text{ cm}^2 \text{ s}^{-1}$ , respectively (Wang et al., 2014). Thus  
 449  $\text{CH}_4$  diffuses into the probe and replenishes the area around the probe more quickly during sampling than  $\text{N}_2\text{O}$ .

450 In System 2, even in soil where controlled soil gas conditions were lacking (i.e. cannot constrain with headspace  
 451 measurement), we observed a decline in measured soil gas concentrations with flow rate, similar to the silica matrix  
 452 experiments (Table 3).

453  
 454  
 455  
 456  
 457  
 458



460 **Figure 11.** Impact of probe sampling flow rate, pore size, trace gas species, and soil matrix on the fractional recovery of true  
 461 soil gas concentrations with probes. Fractional recovery of N<sub>2</sub>O (green) and CH<sub>4</sub> (yellow) in a silica matrix with flowing  
 462 control gas and probe pore size of 10 μm (triangle) and 25 μm (circles). The recovery of N<sub>2</sub>O gas in soil at field moisture (red  
 463 squares), normalized to high recovery, measured with probe pore size 8 μm. All measurements using System 2.

### 464 3.3 Application of sampling system to process studies and interpretation

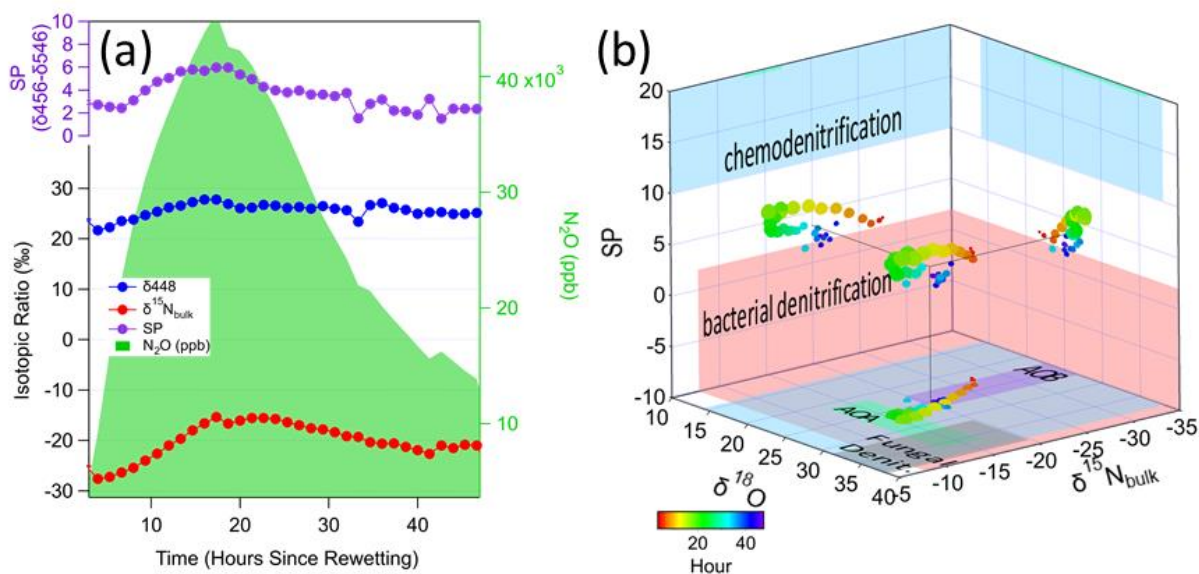
465 Disturbance and environmental variables to soil systems (pedosphere) strongly influence biogeochemical fluxes to  
 466 and from the atmosphere that can be uniquely studied with probes. Following the system optimization (Section 3.2), we no  
 467 longer controlled soil gas concentrations and rather focused on the behavior of real shifts in soil gas recovered by probes,  
 468 which were no longer necessarily reflected by headspace concentrations. In the following tests, we manipulated key drivers of  
 469 soil function (moisture and redox conditions) to elicit responses in soil microbial processes and soil gas concentrations to  
 470 discover the in situ soil gas dynamics newly observable with our soil gas probe sampling system.

#### 471 3.3.1 Impact of soil dry-wet cycle on N<sub>2</sub>O pulse dynamics and process identification (Experiment 5)

472 We used soil trace gas sampling and nitrogen isotopic mapping to identify real-time, in situ changes in N<sub>2</sub>O production  
 473 pathways in response to soil wetting. Soil wetting induced a strong pulse in subsurface N<sub>2</sub>O concentrations, isotopic signatures,  
 474 and site preference that was captured in detail with the N<sub>2</sub>O and CH<sub>4</sub> TILDAS and real time in situ soil gas probe sampling.  
 475 We found that the isotopic ratios of all three N<sub>2</sub>O isotopomers ( $\delta 448$ ,  $\delta 546$ ,  $\delta 456$ ), site preference, and N<sub>2</sub>O concentration  
 476 responded to the wetting over the subsequent 36-hour period. N<sub>2</sub>O rose from approximately 3 ppm to over 40 ppm, with a

477 corresponding and slightly delayed response in isotopic signatures (Fig. 12). The dramatic increase in N<sub>2</sub>O required additional  
 478 dilution at concentrations above the expected range of the TILDAS (>20 ppm). The response of the two <sup>15</sup>N-N<sub>2</sub>O isotopomers  
 479 diverged enough to drive a shift in the site preference (SP) upward by approximately 4‰ to 6‰ before falling back down  
 480 toward 2‰. After the peak, the decline in concentration and isotopic signatures was not explained by soil moisture, which was  
 481 a relatively steady 25-30% volumetric water content (VWC) throughout the period. N<sub>2</sub>O isotopes point to pathways such as  
 482 hydroxylamine decomposition, chemodenitrification, nitrifier denitrification, or denitrifier denitrification. When mapped into  
 483 a 3-dimensional isotope space (Fig. 12b) that is based upon previous observations of SP, <sup>15</sup>N<sub>bulk</sub>, and <sup>18</sup>O for a variety of  
 484 different processes (Toyoda et al., 2017; Wei et al., 2019), the observed isotopic signature falls between chemodenitrification  
 485 and bacterial denitrification. While the <sup>15</sup>N<sub>bulk</sub>, and <sup>18</sup>O signals are dependent upon the substrate <sup>15</sup>N and <sup>18</sup>O compositions, the  
 486 shift over the course of the rewetting measurement indicates a period of more denitrification (at higher SP), then decreasing  
 487 back to bacterial denitrification. Importantly, the observed range of SP values is well below the expected range for bacterial  
 488 and archaeal nitrification (AOB, AOA), which are >20 (off scale in Fig.12b).

489 In contrast to the dynamic response in N<sub>2</sub>O, soil CH<sub>4</sub> concentrations remained low, leading to low signal-to-noise  
 490 ratios in the detected <sup>13</sup>C-CH<sub>4</sub> isotopologue, and did not respond to wetting (data not shown). The dilution rate of the sample  
 491 was increased by 1.9x at hour 18, resulting in a 1.9x reduction in N<sub>2</sub>O concentration measured by the TILDAS (accounted for  
 492 in Fig. 12). Despite the large change in concentration, the isotopic signatures barely changed, even after readjusting the dilution  
 493 rate at hour 42, indicating that their concentration dependence had been well accounted for.



494 **Figure 12.** (a) Soil wetting induced a pulsed response in soil N<sub>2</sub>O (shaded green) and its isotopic signals including δ<sup>448</sup> (blue),  
 495 δ<sup>546</sup> (green), δ<sup>456</sup> (red), and site preference (purple). A soil column without a lid was wetted with the equivalent of 5.1 cm of

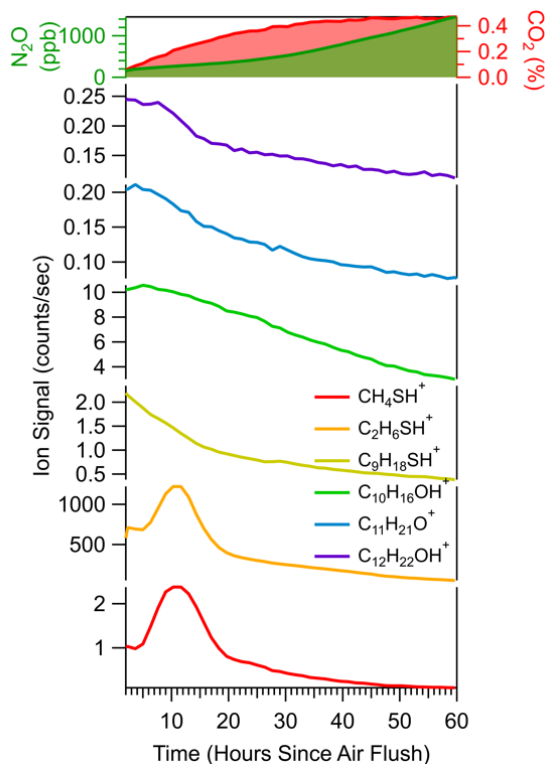
496 rainfall. At 18 hours after wetting the dilution was changed from 2:1 to 3.8:1, and at 41 hours it was changed to 2.1:1, which  
497 is accounted for in the concentrations reported here. (b) Estimated map of N<sub>2</sub>O isotopic signatures of bulk δ<sup>15</sup>N (x-axis), δ<sup>18</sup>O  
498 (y-axis), and site preference (z-axis), circles represent probe measurements of the changes in the isotopic signatures with time  
499 (hours) indicating shifts into region of different microbial activity (colored rectangles) (Table S3). On the x-axis AOA (green  
500 rectangle) and AOB (purple rectangle) refer to nitrification from ammonia oxidizing archaea and ammonia oxidizing bacteria,  
501 respectively. Grey rectangle indicates fungal denitrification.

### 502 3.3.2 Stimulation of subsurface shifts in soil VOC production in response to redox shift (Experiment 6)

503 We measured a diverse suite of soil trace gases including VOCs to determine the consistency of real-time, in situ  
504 changes multiple compounds to shifts in redox from anoxic to oxic conditions in soil. Shifting the soil redox environment from  
505 anoxic to oxic conditions induced a cascade of subsurface gas pulses in CO<sub>2</sub>, N<sub>2</sub>O, and VOCs that we measured by integrating  
506 TILDAS and Vocus analyzers with the real time in situ soil gas probe sampling (Fig. 13). Before this experiment, the soil  
507 column was forced into anoxic conditions by advectively flushing with N<sub>2</sub> through the control gas ports for 3.5 hours;  
508 subsequently, conditions were driven oxic by flushing the system with UZA for a short time at time zero. Conversion to oxic  
509 conditions drove a pulse in N<sub>2</sub>O concentrations that was slow and considerably weaker (reaching 1.6 ppm after 72 hours) than  
510 the wetting response (Experiment 5). The onset of oxic conditions brought a strong CO<sub>2</sub> increase from 0.1 to 0.4%, suggesting  
511 an increase in microbial respiration. Along with CO<sub>2</sub> and N<sub>2</sub>O, we measured a cascade of responses in masses corresponding  
512 to different VOCs. As respiration and nitrogen processing increase, the larger VOCs exhibit either immediate (C<sub>9</sub>H<sub>18</sub>O,  
513 C<sub>11</sub>H<sub>20</sub>O, e.g. nonanal, methylborneol) or delayed loss (C<sub>10</sub>H<sub>16</sub> (monoterpenes), C<sub>12</sub>H<sub>22</sub>O, e.g. geosmin) in the soil. In contrast,  
514 after five hours, the sulfur-containing compounds methanethiol (CH<sub>4</sub>S) and dimethyl sulfide (C<sub>2</sub>H<sub>6</sub>SH) exhibited a surge in  
515 production. The approach captured different sensitivities and temporal responses to a shift in soil redox across a suite of soil  
516 gases that reflect different biochemical processes and their sensitivity to redox conditions.

517

518



519

520 **Figure 13.** A sudden change from anoxic to oxic soil conditions, induced by flushing with UZA, drove dynamic responses in  
 521  $N_2O$ ,  $CO_2$ , and a variety of VOCs captured using the diffusion-based soil probe integrated with the TILDAS and Vocus  
 522 analyzers. System 2 Experiment 6 with a B2 TRF soil sample.

#### 523 4. Discussion

524 We developed a new soil gas sampling system that integrated diffusive sPTFE soil probes with online, high resolution  
 525 trace gas analyzers. The versatile system detected changes in soil concentration and isotopic signatures of  $N_2O$  and  $CH_4$  and  
 526 VOCs that reflected shifting biogeochemical processes in response to environmental manipulation of soil moisture and redox.

#### 527 4.1 Optimizing soil gas sampling

528 Probe sample gas recovery depended on probe flow rate and the trace gas species, while the effect of dilution of the  
 529 probe sample outflow on recovery was minimal. Probe flow rate determines the time available for carrier UZA to equilibrate  
 530 with soil gas across the diffusive membrane as it flows through the probe: lower probe sampling flow rates allow more time  
 531 to equilibrate than do high flow rates (Gut et al., 1998; Parent et al., 2013). By running tests in reverse order, we showed that  
 532 the results were not dependent upon carry-over or memory effects. Correspondingly, we observed that the fractional recovery

533 of true soil gas concentrations declined exponentially with increased probe flow rates across all systems (Fig. 8 and Fig. 11),  
534 analytes (Fig. 7), and probe characteristics tested. The maximum probe flow rates that delivered well-equilibrated samples  
535 (>90% equilibrated) ranged from ~25 to 100 sccm, depending on the system and, in particular, the molecule measured. Indeed,  
536 in both silica and soil matrix, gas recovery was better for molecules with relatively higher molecular diffusivity (i.e. CO, CH<sub>4</sub>,  
537 <sup>12</sup>C-CO<sub>2</sub>) than paired analysis of those with lower diffusivity (i.e. CO<sub>2</sub>, N<sub>2</sub>O, <sup>13</sup>C-CO<sub>2</sub>) (Wang et al., 2014). Molecules with  
538 higher diffusivity move across the membrane and also replenish the area around the probe during sampling more quickly than  
539 those with lower diffusivity. As a result, the upper range of probe flow rates that produce representative gas samples will be  
540 higher for analytes with higher diffusivity, and more restricted for slow diffusing molecules. While isotopic fractionation was  
541 observed in some (CO<sub>2</sub>; Fig. 8), but not all (N<sub>2</sub>O; Fig. 9) tests, incomplete equilibration affected recovery of bulk concentration  
542 more strongly than isotopic signature, suggesting that optimized probe sampling can produce isotopically representative  
543 samples with minimal fractionation. Finally, the representative pore size of sPTFE probes did not correlate with sample  
544 recovery, and all sizes quantitatively recovered >90% of the analyte concentration at optimized flow rates. The sPTFE material  
545 is produced with a characteristic pore size, which may not scale with the total pore density, and could explain the lack of a  
546 pore size dependency across the 5–25 μm range tested.

#### 547 **4.2 Factors yielding a representative sample**

548 One of the challenges in soil trace gas measurements is transferring a representative sample (Parent et al., 2013) from  
549 probes to fill the relatively large sample cell volumes of online analyzers (e.g. 10s to 100s mL at reduced pressure). To address  
550 this issue, we reduced the effective volume of the TILDAS sample cell by designing a more compact cell with a volume-filling  
551 insert (Section 3.1). We also integrated online dilution into the sample transfer system after the probe, which increased the  
552 sample volume delivered to the sample cell without increasing probe flow rates. Dilution also helped reduce soil gas  
553 concentrations to within the range of sensitive trace gas analyzers and avoid condensation (none observed). Together, these  
554 modifications improved the transfer of representative soil gas samples to the cell, increased the cell turnover for a faster time  
555 response, and supported lower probe flow rates for better probe equilibration (Jochheim et al., 2018). Beyond flow-through  
556 sampling, these modifications may be particularly important in future approaches that transfer equilibrated soil gas ‘plugs’ to  
557 an online analyzer for trapped-sample analysis. In addition, reducing sample demand also reduces the disruption of the soil  
558 probe measurement on the soil environment. The diffusive soil probes allow sample gas to diffuse into the probe from the soil  
559 environment, but also allow the UZA carrier gas to diffuse out of the probe into the soil. Under controlled soil conditions  
560 (silica and advective flow), probe sampling caused a < 2% decrease in soil CO<sub>2</sub> concentrations, with a smaller impact at the  
561 low probe flow rates supported by our volume-reducing modifications. In real soil, the impact of carrier diffusion out of the  
562 probe could be larger where local gas concentrations are not replenished by advection but depend on local production,  
563 consumption, and diffusion. In addition to reducing sample volume, lowering the sampling frequency (return rate) may be  
564 especially important for helping to reduce the impact of the perturbation on the soil environment.

### 565 4.3 Transferability to multiple analyzers

566 The continuous online soil gas sampling approach is highly transferable across trace gases and instrument systems.  
567 Here, we successfully measured soil trace gases using two systems. Modifications to reduce sample volume requirements (i.e.,  
568 online dilution, precise flow control, instrument modifications) are transferable to other analyzers beyond the TILDAS  
569 N<sub>2</sub>O/CH<sub>4</sub> isotope analyzer. Although other laser absorption spectroscopy instruments like cavity ringdown spectrometers have  
570 been used to measure concentration and isotopic composition for trace gases like CO<sub>2</sub> (Voglar et al., 2019), TILDAS can  
571 measure several species at high sensitivity/spectral resolution with one instrument (McManus et al., 2015), are field deployable  
572 (McCalley et al., 2014; Roscioli et al., 2015; Saleska et al., 2006), and readily interface with the valving and flow control  
573 system designed here. Some analyzers (e.g., mass spectrometers) are destructive (PTR-MS ionizes molecules for analysis),  
574 preventing the closed-loop scheme sampling from being circulated. However, for other soil gas sampling methods (e.g., online  
575 GC and low-cost sensors) using a closed-loop system continues to be promising approaches to decrease the impact on gas  
576 composition and chemistry during subsurface gas sampling.

577 Not only is the approach transferable across instruments, but we demonstrated that more than one instrument can be  
578 integrated for simultaneous soil probe sampling, e.g. Vocus PTR-TOF-MS for VOCs with the N<sub>2</sub>O/CH<sub>4</sub> TILDAS in parallel  
579 (System 2), and two TILDAS analyzers in series (System 1). This versatility can be extended to allow analysis of a suite of  
580 soil gases using existing TILDAS technology to study, for example, soil microbial N cycling (e.g. N<sub>2</sub>O, NO, NO<sub>2</sub>, NH<sub>3</sub>, HNO<sub>3</sub>,  
581 HONO, NH<sub>2</sub>OH), microbial trace gas scavenging (e.g. CO, OCS, CH<sub>4</sub>, O<sub>2</sub>), and other atmospherically-relevant species (e.g.  
582 H<sub>2</sub>O<sub>2</sub>, HONO, N<sub>2</sub>H<sub>4</sub>, HCHO, HCOOH, CH<sub>3</sub>OH). These compounds represent metabolites for microbial communities, and  
583 intermediates of metabolic pathways of carbon and nitrogen cycling. Coupling these instruments with soil probes will enable  
584 access to incompletely unexplored biological information that reflects metabolic and signaling processes in soil.

### 585 4.4 Considerations for field deployment of the system

586 The sPTFE probes maintained their hydrophobicity, structure, and performance throughout the (> 4 months) of  
587 operation in laboratory soil. In contrast, using silicone membranes, (Panikov et al., 2007) found that the methane calibration  
588 factor differed between a dry and wet membrane. Similarly, (Rothfuss and Conrad, 1994) found memory effect issues when  
589 sampling high concentrations of CH<sub>4</sub> with silicone and epoxy as soil-gas exchange barriers. Soil probes with polypropylene  
590 (PP) membranes have been widely used to measure CO<sub>2</sub> (Gangi et al., 2015; Gut et al., 1998; Jochheim et al., 2018) and  
591 polyethylene (PE) for water isotopes in soil (Volkman and Weiler, 2014; Volkman et al., 2018) and tree xylem (Volkman  
592 et al., 2016a). PP has been successfully used for water isotope analysis (Rothfuss et al., 2013, 2015). However, in our past  
593 experience (T. H. M. Volkman, personal communication) PP and PE probes have shown decreased wall integrity during field  
594 deployment and long term use (i.e., dents and cracks) causing gas and water leaks, compromising hydrophobicity in saturated  
595 media. Importantly, robust performance in this study did not require larger probes; our 15 cm probes were more rigid and

596 smaller than previous probes that were typically 100 to 150 cm in length (Gut et al., 1998; Flechard et al., 2007; Parent et al.,  
597 2013; Rothfuss et al., 2013), and are easily installed via a small drill hole for small-resolution sampling. In some field  
598 applications, it may be more desirable to physically integrate (rather than resolve) variations in soil gas concentrations over a  
599 distance (e.g., for a representative concentration) using a long soil probe, which would help release the low-flow demands of  
600 the relatively short probes used here. Nevertheless, the smaller sPTFE soil probes described have potential to be both less  
601 disruptive to the soil ecosystem and more robust to soil structure and environmental changes for long-term measurements in  
602 the field.

603 The diffusive soil probe sampling system provides a time-dependent picture of soil gas dynamics. This contrasts with  
604 other methods, e.g. manual sampling with syringe (Kammann et al., 2001) and cartridges (Wester- Larsen et al., 2020), that  
605 are more likely to disturb the true soil gas concentration and may compromise sample integrity during transfer for offline  
606 laboratory analysis (Volkman and Weiler, 2014). Manual sampling increases potential measurement error, and is time  
607 consuming and labor intensive, particularly for high temporal or spatial (Wester- Larsen et al., 2020) coverage. Our integrated  
608 sample system can achieve unattended, automated sequential and long-term field soil gas sampling that is less time consuming  
609 and less laborious.

610 In field implementation of our system, there will nevertheless be tradeoffs between sampling frequency and disruption  
611 that should be fully considered. As noted above, diffusive soil sampling can alter soil gas by dilution, and sample transfer  
612 parameters should be optimized to obtain representative samples with minimal disruption. This may be especially important  
613 for distant sampling points that require longer tubing that may release more zero air into the soil during sample transfer to the  
614 analyzer. Therefore, future field studies should consider the biogeochemical implications of adding substrates to the  
615 subsurface, test inert carrier gases like He, and evaluate whether recirculating or flow-through approaches are more appropriate  
616 for each application. The different modules of the sampling system (Fig. 2) are flexible and can be adjusted to accommodate  
617 multiple probes, different measurement specifications, and soil and environmental factors in the field.

#### 618 **4.5 Subsurface gas measurements to capture and interpret environmental drivers of soil processes**

619 Consistent with our technical hypothesis, the optimized soil gas sampling system integrated with the novel N<sub>2</sub>O/CH<sub>4</sub>  
620 TILDAS captured real-time responses in subsurface N<sub>2</sub>O isotopes to a soil wetting event (**Section 3.3.1**). Soil wetting is a  
621 powerful and well-studied driver of biogeochemical change in soils known to result in a rapid release of soil gases (Birch  
622 effect) (Birch, 1958; Leitner et al., 2017) and changes in denitrification emissions of N<sub>2</sub>O (Groffman et al., 2009). The soil  
623 probes, positioned at 20 cm below the soil surface, captured a significant increase in subsurface N<sub>2</sub>O concentration almost  
624 immediately after water was added to the column, and a slow change in isotopic signature that suggests a more gradual change  
625 in the subsurface processing producing N<sub>2</sub>O (Leitner et al., 2017; Van Haren et al., 2005). Our novel subsurface <sup>15</sup>N site  
626 preference measurements showed SP signatures for N<sub>2</sub>O production between those that are characteristic for bacterial

627 denitrification and chemodenitrification pathways (Sutka et al., 2006; Toyoda et al., 2017). As hypothesized, wetting caused  
628 a shift in the N<sub>2</sub>O production pathways relative to the dry condition, and this shift to a higher SP (preferentially enriched on  
629 the central N atom) was short-lived like the N<sub>2</sub>O emission pulse, and relaxed back to pre-wetting levels in less than two days.  
630 These patterns show that the microbial (denitrification) and abiotic (chemodenitrification) pathways vary on long (days) and  
631 short timescales (minutes/hours) at this depth. This information can help guide when to collect soil cores to dig deeper into the  
632 mechanistic drivers through offline analytical approaches.

633 Diverse VOC compounds in the subsurface responded to a shift from soil anoxic to oxic conditions (**Section 3.3.2**).  
634 Redox shifts drive biochemical conversions driven by abiotic reactions (Lin et al., 2021) and microbial respiration or  
635 fermentation metabolism in soil (Peñuelas et al., 2014). As hypothesized, the temporal dynamics of various VOCs and small  
636 molecules (N<sub>2</sub>O, CO<sub>2</sub>) differed, including several fast-responding short-lived pulses and other slow, steady shifts over the 2.5  
637 day measurement period. Numerous microbial metabolic pathways produce volatile molecules that reflect loss in metabolic  
638 pathways and can be difficult to capture with existing metabolomics methods (Honeker et al., 2021; Schulz-Bohm et al., 2015).  
639 Our system displayed the potential to capture hot-moments of trace gas production that did not parallel steady rises in total  
640 microbial activity, for example as reflected by increases in heterotrophic soil respiration (CO<sub>2</sub> emissions) with oxic conditions.  
641 Small molecules and VOCs contribute to soil nutrient cycling, and therefore serve as valuable markers of different and highly  
642 specific microbial activity (Schulz-Bohm et al., 2015). For example geosmin and methylisoborneol are produced by  
643 actinomycetales (Citron et al., 2012; Peñuelas et al., 2014) under anoxic conditions, while sulfurous VOCs are produced in  
644 micro-anoxic sites in soil. Capturing a wide array of volatiles involved in microbial metabolism will increase the understanding  
645 of the impact and role of microbial VOC cycling in pedosphere-atmospheric interactions.

## 646 **5. Conclusion**

647 Versatile trace gas sampling systems that integrate soil probes and high resolution trace gas analyzers bridge an  
648 existing gap in spatial (centimeters) and temporal (minutes) measurements of in situ concentrations and isotopic signatures of  
649 soil trace gases. We demonstrated the feasibility and versatility of an automated multi-probe analysis system for soil gas  
650 measurements of isotopic ratios of nitrous oxide ( $\delta^{18}\text{O}$ ,  $\delta^{15}\text{N}$ , and the <sup>15</sup>N site-preference of N<sub>2</sub>O) and methane ( $\delta^{13}\text{C}$ ), and  
651 VOCs, all important gas-phase indicators of biological activity. This study showed that (1) the system has the potential to be  
652 used with other gas and isotope analyzers, (2) there was no evidence of any interference during the TILDAS-PTR-MS Vocus  
653 inline measurements, and (3) the nitrous oxide analyzer configuration achieved a reduced concentration dependency allowing  
654 determination of N<sub>2</sub>O isotopic measurements over a larger range in concentration. Importantly, the sampling system captured  
655 fluctuations in subsurface gas concentrations and isotopologues in response to rapid changes in environmental conditions.  
656 Specifically, revealing dynamics of microbial metabolism that drive hot moments of gas emissions under variable soil moisture

657 and redox conditions. These tests demonstrate the potential of this approach to reveal interconnections between the soil  
658 microbiome, its local environment, and the atmosphere.

659  
660 The outlook is bright for integrating soil gas measurements with other data and models to unlock new understanding  
661 of soil microbial processes. Direct sampling of soil for subsequent laboratory incubations and analysis using multi-omic  
662 approaches is a sensitive and precise approach for identifying subsurface microbial populations and their potential metabolic  
663 function. Although both widely used approaches produce reliable and robust results, they are labor intensive and destructive,  
664 and incompatible with generating a well resolved spatial- and time-dependent understanding of microbial activity in natural  
665 ecosystems. Similarly, current soil gas sampling methodologies face challenges to address the gap between time-space  
666 sampling (e.g. frequency and intensity), low bias in downstream analysis, and proper reference materials. Isotopic signatures  
667 of trace soil gases, in conjunction with genomic and metabolomics approaches can elucidate real time biomarkers of microbial  
668 metabolisms in soil, leading to a better understanding of soil heterogeneity as a modulator of soil-microbe interactions and  
669 their responses to environmental factors and nutrient cycling. These efforts will help scale up soil trace gases monitoring and  
670 quantification of biogeochemical processes to improve soil modeling, soil management decisions, and soil health with high  
671 spatial and temporal resolution.

672 **Data availability.** Igor software was used under license. Igor scripts were used for data processing and analysis including  
673 Aerodyne Research Inc. proprietary scripts for parsing and averaging data and cannot be in a public repository. Other portions  
674 of Igor code used for plotting are available upon request. Raw measurements files (e.g., TILDAS and vocus spectra) will be  
675 available upon request. Processed data can be found at DOI: 10.25422/azu.data.13383014

676 **Supplement.** Additional supporting information available online at:

677 **Author contribution.** All authors made substantial contributions to the research. T.H.M.V, L.K.M., J.R.R., J.H.S.  
678 conceptualized the idea and acquired funding. All authors participated in part or all of developing prototypes, building  
679 experimental systems, and conducting experiments. J.G.L, L.K.M., J.R.R., J.H.S. contributed to the analyses and interpretation  
680 of data; J.G.L. and L.K.M. prepared the draft, all authors discussed the results and contributed to the final manuscript.

681 **Acknowledgments.** This material is based upon work supported by the U.S. Department of Energy, Office of Science, Office  
682 of The Small Business Innovation Research (SBIR) grant, Office of Science, under Award Number(s) DE-SC0018459. THMV  
683 was supported by Biosphere 2 through the office of the Senior Vice President for Research Innovation and Impact at the  
684 University of Arizona. We thank Doug White and White Industries, Inc. for machining the probes. The authors gratefully  
685 acknowledge financial support from the Phileology Foundation for Biosphere 2 and the Landscape Evolutionary Observatory.  
686 Prof. Shuhei Ono at the Massachusetts Institute of Technology has shared with us calibrated reference gases for this study.

687 **Conflicts of Interest.** Aerodyne Research Inc manufactures the TILDAS instrumentation and commercializes the Vocus PTR-  
688 TOF for applications in geosciences. Probes, sampling systems and associated software are in development.

689 Disclaimer: *"This report was prepared as an account of work sponsored by an agency of the United States*  
690 *Government. Neither the United States Government nor any agency thereof, nor any of their employees, makes any warranty,*  
691 *express or implied, or assumes any legal liability or responsibility for the accuracy, completeness, or usefulness of any*  
692 *information, apparatus, product, or process disclosed, or represents that its use would not infringe privately owned rights.*  
693 *Reference herein to any specific commercial product, process, or service by trade name, trademark, manufacturer, or*  
694 *otherwise does not necessarily constitute or imply its endorsement, recommendation, or favoring by the United States*  
695 *Government or any agency thereof. The views and opinions of authors expressed herein do not necessarily state or reflect*  
696 *those of the United States Government or any agency thereof."*

## 697 **References**

- 698 [Abis, L., Loubet, B., Ciuraru, R., Lafouge, F., Houot, S., Nowak, V., Tripied, J., Dequiedt, S., Maron, P. A., and Sadet-  
699 Bourgeteau, S.: Reduced microbial diversity induces larger volatile organic compound emissions from soils, \*Sci. Rep.\*, 10,  
700 6104, 2020.](#)
- 701 [Birch, H. F.: The effect of soil drying on humus decomposition and nitrogen availability, \*Plant Soil\*, 10, 9–31, 1958.](#)
- 702 [Burton, D. L. and Beauchamp, E. G.: Profile nitrous oxide and carbon dioxide concentrations in a soil subject to freezing,  
703 \*Soil Sci. Soc. Am. J.\*, 58, 115–122, 1994.](#)
- 704 [Bzowski, J., Kestin, J., Mason, E. A., and Uribe, F. J.: Equilibrium and Transport Properties of Gas Mixtures at Low  
705 Density: Eleven Polyatomic Gases and Five Noble Gases, \*J. Phys. Chem. Ref. Data\*, 19, 1179–1232, 1990.](#)
- 706 [Citron, C. A., Gleitzmann, J., Laurenzano, G., Pukall, R., and Dickschat, J. S.: Terpenoids are widespread in actinomycetes:  
707 a correlation of secondary metabolism and genome data, \*Chembiochem\*, 13, 202–214, 2012.](#)
- 708 [Clough, T. J., Kelliher, F. M., Wang, Y. P., and Sherlock, R. R.: Diffusion of <sup>15</sup>N-labelled N<sub>2</sub>O into soil columns: a  
709 promising method to examine the fate of N<sub>2</sub>O in subsoils, \*Soil Biol. Biochem.\*, 38, 1462–1468, 2006.](#)
- 710 [Conrad, R.: Quantification of methanogenic pathways using stable carbon isotopic signatures: a review and a proposal, \*Org.\*  
711 \*Geochem.\*, 36, 739–752, 2005.](#)
- 712 [DeSutter, T. M., Sauer, T. J., and Parkin, T. B.: Porous tubing for use in monitoring soil CO<sub>2</sub> concentrations, \*Soil Biol.\*  
713 \*Biochem.\*, 38, 2676–2681, 2006.](#)
- 714 [Dhanumalayan, E. and Joshi, G. M.: Performance properties and applications of polytetrafluoroethylene \(PTFE\)—a review  
715 \*Adv. Compos. Hybr. Mater.\*, 1, 247–268, 2018.](#)
- 716 [Flechard, C. R., Neftel, A., Jocher, M., Ammann, C., Leifeld, J., and Fuhrer, J.: Temporal changes in soil pore space CO<sub>2</sub>  
717 concentration and storage under permanent grassland, \*Agric. For. Meteorol.\*, 142, 66–84, 2007.](#)
- 718 [Gangi, L., Rothfuss, Y., Ogée, J., Wingate, L., Vereecken, H., and Brüggemann, N.: A New Method for In Situ  
719 Measurements of Oxygen Isotopologues of Soil Water and Carbon Dioxide with High Time Resolution, \*Vadose Zone J.\*, 14,](#)

- 720 [vzj2014.11.0169](#), 2015.
- 721 Gonzalez-Meler, M. A., Rucks, J. S., and Aubanell, G.: Mechanistic insights on the responses of plant and ecosystem gas  
722 exchange to global environmental change: lessons from Biosphere 2, *Plant Sci.*, 226, 14–21, 2014.
- 723 Groffman, P. M., Butterbach-Bahl, K., Fulweiler, R. W., Gold, A. J., Morse, J. L., Stander, E. K., Tague, C., Tonitto, C., and  
724 Vidon, P.: Challenges to incorporating spatially and temporally explicit phenomena (hotspots and hot moments) in  
725 denitrification models, *Biogeochemistry*, 93, 49–77, 2009.
- 726 Guenther, A., Hewitt, C. N., Erickson, D., Fall, R., Geron, C., Graedel, T., Harley, P., Klinger, L., Lerdau, M., Mckay, W.  
727 A., Pierce, T., Scholes, B., Steinbrecher, R., Tallamraju, R., Taylor, J., and Zimmerman, P.: A global model of natural  
728 volatile organic compound emissions, *J. Geophys. Res.*, 100, 8873, 1995.
- 729 Gut, A., Blatter, A., Fahrni, M., Lehmann, B. E., Neftel, A., and Staffelbach, T.: A new membrane tube technique (METT)  
730 for continuous gas measurements in soils, *Plant Soil*, 198, 79–88, 1998.
- 731 Hirsch, A. I., Trumbore, S. E. and Goulden, M. L.: The surface CO<sub>2</sub> gradient and pore-space storage flux in a high-porosity  
732 litter layer, *Tellus B Chem Phys Meteorol*, 56(4), 312–321, doi:10.3402/tellusb.v56i4.16449, 2004.
- 733 Holter, P.: Sampling air from dung pats by silicone rubber diffusion chambers, *Soil Biol. Biochem.*, 22, 995–997, 1990.
- 734 Honeker, L. K., Graves, K. R., Tfaily, M. M., Krechmer, J. E., and Meredith, L. K.: The volatilome: A vital piece of the  
735 complete soil metabolome, *Front. Environ. Sci.*, 9, <https://doi.org/10.3389/fenvs.2021.649905>, 2021.
- 736 Insam, H. and Seewald, M. S. A.: Volatile organic compounds (VOCs) in soils, *Biol. Fertil. Soils*, 46, 199–213, 2010.
- 737 Jacinthe, P.-A. and Dick, W. A.: Use of silicone tubing to sample nitrous oxide in the soil atmosphere, *Soil Biol. Biochem.*,  
738 28, 721–726, 1996.
- 739 Jiao, S., Chen, W., Wang, J., Du, N., Li, Q., and Wei, G.: Soil microbiomes with distinct assemblies through vertical soil  
740 profiles drive the cycling of multiple nutrients in reforested ecosystems, *Microbiome*, 6, 146, 2018.
- 741 Jochheim, H., Wirth, S., and von Unold, G.: A multi-layer, closed-loop system for continuous measurement of soil CO<sub>2</sub>  
742 concentration, *J. Plant Nutr. Soil Sci.*, 181, 61–68, 2018.
- 743 [Kammann, C., Grünhage, L., and Jäger, H.-J.: A new sampling technique to monitor concentrations of CH<sub>4</sub>, N<sub>2</sub>O and CO<sub>2</sub> in  
744 air at well-defined depths in soils with varied water potential, \*Eur. J. Soil Sci.\*, \[https://doi.org/10.1046/j.1365-  
2389.2001.00380.x\]\(https://doi.org/10.1046/j.1365-<br/>745 2389.2001.00380.x\), 2001.](#)
- 746 Karbin, S., Guillet, C., Kammann, C. I., and Niklaus, P. A.: Effects of Long-Term CO<sub>2</sub> Enrichment on Soil-Atmosphere  
747 CH<sub>4</sub> Fluxes and the Spatial Micro-Distribution of Methanotrophic Bacteria, *PLoS One*, 10, e0131665, 2015.
- 748 Krämer, H. and Conrad, R.: Measurement of dissolved H<sub>2</sub> concentrations in methanogenic environments with a gas  
749 diffusion probe, *FEMS Microbiol. Ecol.*, 12, 149–158, 1993.
- 750 Krechmer, J., Lopez-Hilfiker, F., Koss, A., Hutterli, M., Stoermer, C., Deming, B., Kimmel, J., Warneke, C., Holzinger, R.,  
751 Jayne, J., Worsnop, D., Fuhrer, K., Gonin, M., and de Gouw, J.: Evaluation of a New Reagent-Ion Source and Focusing Ion-  
752 Molecule Reactor for Use in Proton-Transfer-Reaction Mass Spectrometry, *Anal. Chem.*, 90, 12011–12018, 2018.
- 753 Laemmel, T., Maier, M., Schack-Kirchner, H., and Lang, F.: An in situ method for real-time measurement of gas transport in  
754 soil : Monitoring of gas transport in soil, *Eur. J. Soil Sci.*, 68, 156–166, 2017.
- 755 Leitner, S., Homyak, P. M., Blankinship, J. C., Eberwein, J., Jenerette, G. D., Zechmeister-Boltenstern, S., and Schimel, J.

- 756 P.: Linking NO and N<sub>2</sub>O emission pulses with the mobilization of mineral and organic N upon rewetting dry soils, *Soil Biol. Biochem.*, 115, 461–466, 2017.
- 757
- 758 Lin, Y., Campbell, A. N., Bhattacharyya, A., DiDonato, N., Thompson, A. M., Tfaily, M. M., Nico, P. S., Silver, W. L., and Pett-Ridge, J.: Differential effects of redox conditions on the decomposition of litter and soil organic matter, *Biogeochemistry*, <https://doi.org/10.1007/s10533-021-00790-y>, 2021.
- 759
- 760
- 761 Maier, M., Schack-Kirchner, H., Aubinet, M., Goffin, S., Longdoz, B., and Parent, F.: Turbulence Effect on Gas Transport in Three Contrasting Forest Soils, *Soil Sci. Soc. Am. J.*, 76, 1518–1528, 2012.
- 762
- 763 Massman, W. J.: A review of the molecular diffusivities of H<sub>2</sub>O, CO<sub>2</sub>, CH<sub>4</sub>, CO, O<sub>3</sub>, SO<sub>2</sub>, NH<sub>3</sub>, N<sub>2</sub>O, NO, and NO<sub>2</sub> in air, O<sub>2</sub> and N<sub>2</sub> near STP, *Atmos. Environ.*, [https://doi.org/10.1016/s1352-2310\(97\)00391-9](https://doi.org/10.1016/s1352-2310(97)00391-9), 1998.
- 764
- 765 **MATLAB**, 2018. 9.7.0.1190202 (R2019b), Natick, Massachusetts: The MathWorks Inc.
- 766 McCalley, C. K., Woodcroft, B. J., Hodgkins, S. B., Wehr, R. A., Kim, E.-H., Mondav, R., Crill, P. M., Chanton, J. P., Rich, V. I., Tyson, G. W., and Saleska, S. R.: Methane dynamics regulated by microbial community response to permafrost thaw, *Nature*, 514, 478–481, 2014.
- 767
- 768
- 769 McClellan, M. J.: Estimating regional nitrous oxide emissions using isotopic ratio observations and a Bayesian inverse framework, Ph.D, Massachusetts Institute of Technology. [online] Available from: <https://dspace.mit.edu/handle/1721.1/119986> (Accessed 8 September 2020), 2018.
- 770
- 771
- 772 McManus, J. B., Nelson, D. D., and Zahniser, M. S.: Design and performance of a dual-laser instrument for multiple isotopologues of carbon dioxide and water, *Opt. Express*, 23, 6569–6586, 2015.
- 773
- 774 McSharry, C., Faulkner, R., Rivers, S., Shaffer, M. S. P., and Welton, T.: The chemistry of East Asian lacquer: A review of the scientific literature, *Stud Conserv*, 52, 29–40, 2007.
- 775
- 776 Mohn, J., Wolf, B., Toyoda, S., Lin, C.-T., Liang, M.-C., Brüggemann, N., Wissel, H., Steiker, A. E., Dyckmans, J., Szvec, L., Ostrom, N. E., Casciotti, K. L., Forbes, M., Giesemann, A., Well, R., Doucett, R. R., Yarnes, C. T., Ridley, A. R., Kaiser, J., and Yoshida, N.: Interlaboratory assessment of nitrous oxide isotopomer analysis by isotope ratio mass spectrometry and laser spectroscopy: current status and perspectives, *Rapid Commun. Mass Spectrom.*, 28, 1995–2007, 2014.
- 777
- 778
- 779
- 780 Munksgaard, N. C., Wurster, C. M., and Bird, M. I.: Continuous analysis of  $\delta^{18}\text{O}$  and  $\delta\text{D}$  values of water by diffusion sampling cavity ring-down spectrometry: a novel sampling device for unattended field monitoring of precipitation, ground and surface waters, *Rapid Commun. Mass Spectrom.*, <https://doi.org/10.1002/rcm.5282>, 2011.
- 781
- 782
- 783 Panikov, N. S., Mastepanov, M. A., and Christensen, T. R.: Membrane probe array: Technique development and observation of CO<sub>2</sub> and CH<sub>4</sub> diurnal oscillations in peat profile, *Soil Biol. Biochem.*, 39, 1712–1723, 2007.
- 784
- 785 Parent, F., Plain, C., Epron, D., Maier, M., and Longdoz, B.: A new method for continuously measuring the  $\delta^{13}\text{C}$  of soil CO<sub>2</sub> concentrations at different depths by laser spectrometry, *Eur. J. Soil Sci.*, <https://doi.org/10.1111/ejss.12047>, 2013.
- 786
- 787 Penger, J., Conrad, R., and Blaser, M.: Stable carbon isotope fractionation by methylotrophic methanogenic archaea, *Appl. Environ. Microbiol.*, 78, 7596–7602, 2012.
- 788
- 789 Peñuelas, J., Asensio, D., Tholl, D., Wenke, K., Rosenkranz, M., Piechulla, B., and Schnitzler, J. P.: Biogenic volatile emissions from the soil, *Plant Cell Environ.*, 37, 1866–1891, 2014.
- 790
- 791 Petersen, S. O.: Diffusion probe for gas sampling in undisturbed soil, *Eur. J. Soil Sci.*, 65, 663–671, 2014.
- 792 Raza, W., Mei, X., Wei, Z., Ling, N., Yuan, J., Wang, J., Huang, Q., and Shen, Q.: Profiling of soil volatile organic

- 793 compounds after long-term application of inorganic, organic and organic-inorganic mixed fertilizers and their effect on plant  
794 growth, *Sci. Total Environ.*, 607-608, 326–338, 2017.
- 795 Rock, L., Ellert, B. H., Mayer, B., and Norman, A. L.: Isotopic composition of tropospheric and soil N<sub>2</sub>O from successive  
796 depths of agricultural plots with contrasting crops and nitrogen amendments, *J. Geophys. Res. D: Atmos.*, 112,  
797 <https://doi.org/10.1029/2006JD008330>, 2007.
- 798 Roscioli, J. R., Yacovitch, T. I., Floerchinger, C., Mitchell, A. L., Tkacik, D. S., Subramanian, R., Martinez, D. M., Vaughn,  
799 T. L., Williams, L., Zimmerle, D., and Others: Measurements of methane emissions from natural gas gathering facilities and  
800 processing plants: measurement methods, *Atmos. Meas. Tech.*, 8(5), <https://doi.org/10.5194/amt-8-2017-2015>, 2015.
- 801 Rothfuss, F. and Conrad, R.: Development of a gas diffusion probe for the determination of methane concentrations and  
802 diffusion characteristics in flooded paddy soil, *FEMS Microbiol. Ecol.*, 14, 307–318, 1994.
- 803 Rothfuss, Y., Vereecken, H., and Brüggemann, N.: Monitoring water stable isotopic composition in soils using gas-  
804 permeable tubing and infrared laser absorption spectroscopy, *Water Resour. Res.*, <https://doi.org/10.1002/wrcr.20311>, 2013.
- 805 Rothfuss, Y., Merz, S., Vanderborght, J., Hermes, N., Weuthen, A., Pohlmeier, A., Vereecken, H., and Brüggemann, N.:  
806 Long-term and high-frequency non-destructive monitoring of water stable isotope profiles in an evaporating soil column,  
807 *Hydrol. Earth Syst. Sci.*, <https://doi.org/10.5194/hess-19-4067-2015>, 2015.
- 808 Rothman, L. S., Gordon, I. E., Babikov, Y., Barbe, A., Benner, D. C., Bernath, P. F., Birk, M., Bizzocchi, L., Boudon, V.,  
809 Brown, L. R., and Others: The HITRAN2012 molecular spectroscopic database, *J. Quant. Spectrosc. Radiat. Transf.*, 130, 4–  
810 50, 2013.
- 811 Saleska, S. R., Shorter, J. H., Herndon, S., Jiménez, R., Barry McManus, J., William Munger, J., Nelson, D. D., and  
812 Zahniser, M. S.: What are the instrumentation requirements for measuring the isotopic composition of net ecosystem  
813 exchange of CO<sub>2</sub> using eddy covariance methods?, *Isot. Environ. Health Stud.*, <https://doi.org/10.1080/10256010600672959>,  
814 2006.
- 815 Schimel, J. P.: Life in Dry Soils: Effects of Drought on Soil Microbial Communities and Processes, *Annu. Rev. Ecol. Evol.*  
816 *Syst.*, <https://doi.org/10.1146/annurev-ecolsys-110617-062614>, 2018.
- 817 Schulz-Bohm, K., Zweepers, H., de Boer, W., and Garbeva, P.: A fragrant neighborhood: volatile mediated bacterial  
818 interactions in soil, *Front. Microbiol.*, 6, 1212, 2015.
- 819 Schulz-Bohm, K., Gerards, S., Hundscheid, M., Melenhorst, J., de Boer, W., and Garbeva, P.: Calling from distance:  
820 attraction of soil bacteria by plant root volatiles, *ISME J.*, 12, 1252–1262, 2018.
- 821 Snider, D. M., Venkiteswaran, J. J., Schiff, S. L., and Spoelstra, J.: From the Ground Up: Global Nitrous Oxide Sources are  
822 Constrained by Stable Isotope Values, *PLOS ONE*, <https://doi.org/10.1371/journal.pone.0118954>, 2015.
- 823 Sutka, R. L., Ostrom, N. E., Ostrom, P. H., Breznak, J. A., Gandhi, H., Pitt, A. J., and Li, F.: Distinguishing nitrous oxide  
824 production from nitrification and denitrification on the basis of isotopomer abundances, *Appl. Environ. Microbiol.*, 72, 638–  
825 644, 2006.
- 826 Team, R. C.: R Core Team (2017). R: A language and environment for statistical computing, 2017.
- 827 Toyoda, S., Yoshida, N., and Koba, K.: Isotopocule analysis of biologically produced nitrous oxide in various environments,  
828 *Mass Spectrom. Rev.*, 36, 135–160, 2017.
- 829 Van Haren, J. L. M., Handley, L. L., Biel, K. Y., Kudeyarov, V. N., McLain, J. E. T., Martens, D. A., and Colodner, D. C.:

- 830 Drought-induced nitrous oxide flux dynamics in an enclosed tropical forest, *Glob. Chang. Biol.*, 11, 1247–1257, 2005.
- 831 Voglar, G. E., Zavadlav, S., Levanič, T., and Ferlan, M.: Measuring techniques for concentration and stable isotopologues of  
832 CO<sub>2</sub> in a terrestrial ecosystem: A review, *Earth-Sci. Rev.*, 199, 102978, 2019.
- 833 Volkman, T. H. M. and Weiler, M.: Continual in situ monitoring of pore water stable isotopes in the subsurface, *Hydrol.*  
834 *Earth Syst. Sci.*, 18, 1819–1833, 2014.
- 835 Volkman, T. H. M., Kühnhammer, K., Herbstritt, B., Gessler, A., and Weiler, M.: A method for in situ monitoring of the  
836 isotope composition of tree xylem water using laser spectroscopy, *Plant, Cell & Environ.*, <https://doi.org/10.1111/pce.12725>,  
837 2016a.
- 838 Volkman, T. H. M., Haberer, K., Gessler, A., and Weiler, M.: High-resolution isotope measurements resolve rapid  
839 ecohydrological dynamics at the soil plant interface, *New Phytol.*, 210, 839–849, 2016b.
- 840 Volkman, T. H. M., Sengupta, A., Pangle, L. A., Dontsova, K., Barron-Gafford, G. A., Harman, C. J., Niu, G.-Y.,  
841 Meredith, L. K., Abramson, N., Neto, A. A. M., and Others: Controlled experiments of hillslope coevolution at the  
842 Biosphere 2 Landscape Evolution Observatory: Toward prediction of coupled hydrological, biogeochemical, and ecological  
843 change, in: *Hydrology of Artificial and Controlled Experiments*, edited by: Jiu-Fu Liu, W.-Z. G., IntechOpen, 25–74, 2018.
- 844 Wang, Y., Hu, C., Ming, H., Oenema, O., Schaefer, D. A., Dong, W., Zhang, Y., and Li, X.: Methane, Carbon Dioxide and  
845 Nitrous Oxide Fluxes in Soil Profile under a Winter Wheat-Summer Maize Rotation in the North China Plain, *PLoS ONE*,  
846 <https://doi.org/10.1371/journal.pone.0098445>, 2014.
- 847 Wei, J., Ibraim, E., Brüggemann, N., Vereecken, H., and Mohn, J.: First real-time isotopic characterisation of N<sub>2</sub>O from  
848 chemodenitrification, *Geochim. Cosmochim. Acta*, 267, 17–32, 2019.
- 849 Werle, P., Mucke, R., and Slemr, F.: The limits of signal averaging in atmospheric trace-gas monitoring by tunable diode-  
850 laser absorption spectroscopy (TDLAS), *Applied Physics B*, <https://doi.org/10.1007/bf00425997>, 1993.
- 851 Wester- Larsen, L., Kramshøj, M., Albers, C. N., and Rinnan, R.: Biogenic Volatile Organic Compounds in Arctic Soil: A  
852 Field Study of Concentrations and Variability With Vegetation Cover, *J. Geophys. Res. Biogeosci.*, 125, 36, 2020.
- 853 Yoshida, N. and Toyoda, S.: Constraining the atmospheric N<sub>2</sub>O budget from intramolecular site preference in N<sub>2</sub>O  
854 isotopomers, *Nature*, 405, 330–334, 2000.
- 855
- 856